The stratigraphic record of continental breakup, offshore NW Australia

Matthew T. Reeve[1], Craig Magee[1,2]*, Christopher A-L. Jackson[1,3], Rebecca E. Bell[1], Ian D. Bastow[1]

[1]Basins Research Group (BRG), Department of Earth Science and Engineering, Imperial College London, SW7 2BP, England, UK
[2]School of Earth and Environment, University of Leeds, Leeds, LS2 9JT, UK
[3]Department of Earth and Environmental Sciences, University of Manchester, Williamson Building, Oxford Road, Manchester, M13 9PL, UK

*corresponding author: Craig Magee (c.magee@leeds.ac.uk)

Abstract

Continental breakup involves a transition from rapid, fault-controlled syn-rift subsidence to relatively slow, post-breakup subsidence induced lithospheric cooling. Yet the stratigraphic record of many rifted margins contain syn-breakup unconformities, indicating episodes of uplift and erosion interrupt this transition. This uplift has been linked to mantle upwelling, depth-dependent extension, and/or isostatic rebound. Deciphering the breakup processes recorded by these unconformities and their related rock record is difficult because associated erosion commonly removes the strata that help constrain the onset and duration of uplift. We examine three major breakup-related unconformities and intervening rock record in the Lower Cretaceous succession of the Gascoyne and Cuvier margins, offshore NW Australia, using seismic reflection and borehole data. These data show the breakup unconformities are disconformable (non-erosive) in places and angular (erosive) in others. Our recalibration of palynomorph ages from rocks underlying and overlying the unconformities shows: (i) the lowermost unconformity developed between 134.98–133.74 Ma (Intra-Valanginian), probably during the localisation of magma intrusion within continental crust and consequent formation of continent-ocean transition zones (COTZ); (2) the middle unconformity formed between ~134–133 Ma (Top Valanginian), possibly coincident with breakup of continental crust and generation of new magmatic (but not oceanic) crust within the COTZs; and (iii) the uppermost unconformity likely developed between ~132.5–131 Ma (i.e. Intra-Hauterivian), coincident with full breakup of continental lithosphere and the onset of seafloor spreading. During unconformity formation, uplift was focused along the continental rift flanks, likely reflecting landward flow of lower crustal and/or lithospheric mantle from beneath areas of localised extension towards the continent (i.e. depth-dependent extension). Our work supports the growing consensus that the 'breakup unconformity' is not always a single stratigraphic surface marking the onset of seafloor spreading; multiple unconformities may form and reflect a complex history of uplift and subsidence during the development of continent-ocean transition.

1. Introduction

Continental breakup has traditionally been perceived to involve continuous subsidence of an evolving rifted margin, with initial fault-controlled, relatively rapid syn-rift subsidence followed by a protracted phase of relatively slow, post-rift subsidence induced by cooling of the lithosphere (e.g., McKenzie 1978; Le Pichon & Sibuet 1981; Bott 1982). However, the stratigraphic records of many passive margins contain one or more 'breakup unconformities' (Fig. 1), which developed sub-aerially during the transition from continental rifting to seafloor spreading (e.g., Falvey 1974; Veevers 1986; Driscoll et al. 1995; Lavin 1997; Tucholke et al. 2007; Soares et al. 2012; Franke 2013; Mohriak & Leroy 2013; Morley 2016;

Gong et al. 2019; Xie et al. 2019). These breakup unconformities broadly separate faulted, syn-rift rocks from overlying, largely unfaulted post-rift rocks, indicating subsidence was punctuated by a period of margin-wide uplift and/or erosion (e.g., Falvey 1974; Embry & Dixon 1990; Driscoll et al. 1995; Alves & Cunha 2018; Pérez-Gussinyé et al. 2020). Such syn-breakup uplift has variously been attributed to: (i) a thermal response to mantle upwelling (e.g., Falvey 1974; Morley 2016); (ii) rift flank uplift caused either by convective heat transfer from deeper parts of a rifted basin (e.g., Cochran 1983), or an isostatic response to depth-dependent extension (e.g., White & McKenzie 1988; Issler et al. 1989); or (iii) isostatic rebound of over-deepened sedimentary basins (e.g., Braun & Beaumont 1989). The magnitude and distribution of uplift is also influenced by lithospheric strength (see Pérez-Gussinyé et al. 2020 and references therein). The stratigraphic architecture and formation of these unconformities and their encasing strata, i.e. the breakup sequence, thus provides an important record of the tectonic and geodynamic evolution of continental margins (e.g., Soares et al. 2012; Alves & Cunha 2018; Gong et al. 2019; Monteleone et al. 2019; Peron-Pinvidic et al. 2019; Pérez-Gussinyé et al. 2020).

To understand the genesis and significance of breakup-related unconformities, we must establish their distribution and structure, the depositional environments and subsidence history of a margin, and the timing of unconformity development relative to distinct tectonic and magmatic events (e.g., full lithospheric rupture and onset of seafloor spreading). Most previous studies investigating the development and geodynamic significance of breakup unconformities are limited by: (i) seismic and borehole data quantity and quality (e.g., Soares et al. 2012); (ii) paucity of biostratigraphic constraints on the age of the breakup succession, particularly where erosion has removed rock beneath related unconformities (e.g., Dafoe et al. 2017); (iii) poor dating of oceanic crust adjacent to the margin, which makes it difficult to establish whether unconformity development and onset of seafloor spreading were simultaneous (e.g., Cande & Mutter 1982); (iv) complications due to diachronous breakup along-strike and the formation of multiple breakup unconformities (e.g., Larsen & Saunders 1998; Soares et al. 2012; Gillard et al. 2015; Alves & Cunha 2018; Monteleone et al. 2019); or (v) the presence of substantial syn-breakup igneous products, which tends to reduce the quality of seismic reflection data (e.g., Skogseid et al. 1992).

The North Carnarvon Basin, offshore NW Australia (Fig. 2), is an ideal area to understand the syn-breakup stratigraphic record and thereby determine mechanisms of continental breakup. We use 2D and 3D reflection seismic surveys covering ~165,000 km^2 and biostratigraphic data from 165 boreholes to better constrain the age and uplift distribution of three major unconformities that have previously dated to 138.2 Ma, 134.9 Ma, and ~132.5 Ma (e.g., Helby et al. 1987; Arditto 1993; Labutis 1994; Smith et al. 2015; Paumard et al. 2018). Developing previous work, a recent examination of the nature and age of the Cuvier Abyssal Plain, adjacent to part of the North Carnarvon Basin, has shown continental breakup of NW Australia involved a protracted (~6 Myr) period of continent-ocean transition zone (COTZ) formation immediately before full lithospheric rupture occurred ~130 Ma (Reeve et al. 2021). Although the three unconformities studied here have been broadly linked to continental breakup (e.g., Helby et al. 1987; Arditto 1993; Labutis 1994; Smith et al. 2015; Paumard et al. 2018), the tectonic processes driving their formation remain poorly understood. By recalibrating widely preserved dinoflagellate zones to align with sparse, yet temporally well-constrained occurrences of calcareous nannofossils, we show the three unconformities actually developed between 134.98–133.74 Ma, ~134–133 Ma, and ~132.5–131 Ma. Mapping the age, depositional environment, and reworking of sedimentary rocks above and below the major breakup-related unconformities reveals uplift was primarily focused along rift flanks bordering continent-ocean transition zones (COTZs). We compare these constraints on unconformity development to the structure and magnetic stripe ages recorded in neighbouring Early Cretaceous COTZs and oceanic crust. Based on these comparisons, we suggest that the three phases of uplift and unconformity development coincided with: (i) formation of narrow rift zones, which involved significant dyke intrusion into continental crust; (ii) possible initiation of dyke-driven, sub-aerial spreading, and the formation of new magmatic crust (i.e. marking breakup of continental crust); and (iii) onset of full lithospheric breakup and seafloor spreading. We speculate uplift and erosion occurred in response to the landward transfer of lower crustal and/or lithospheric material to beneath the rift flanks from areas where extension became localised. Overall, our work shows that the integration of seismic reflection and well-calibrated biostratigraphic data is critical to reading rocks that record the processes driving continental breakup.

2. Geological setting

The Palaeozoic-to-Recent North Carnarvon Basin forms the southern-most part of Australia's Northwest Shelf, spanning the magma-rich Gascoyne and Cuvier margins (Fig. 2) (e.g., Symonds et al. 1998; Longley et al. 2002; Menzies et al. 2002). The basin developed in response to multiple phases of rifting between the Late Carboniferous and Early Cretaceous, with internal sub-basins developing from the Late Triassic onwards (e.g., Stagg & Colwell 1994; Longley et al. 2002). In this study, we principally consider the Tithonian-to-Hauterivian phase of rifting that led to continental breakup between Australia and Greater India (Fig. 3A) (e.g., Falvey & Veevers 1974; Willcox & Exon 1976; Larson et al. 1979; Stagg & Colwell 1994; Longley et al. 2002; Stagg et al. 2004; Heine & Müller 2005; Robb et al. 2005; Direen et al. 2008; Reeve et al. 2021).

2.1. Margin sectors

2.1.1. Gascoyne Margin

The 450–700 km wide Gascoyne Margin contains a 100–250 km wide COTZ that hosts magnetic chrons M10N–M5n (135.9–130.6 Ma), and to the south-west is separated from the Cuvier Abyssal Plain by the NW-trending Cape Range Fracture Zone (Fig. 2A) (e.g., Direen et al. 2008). The oldest magnetic anomaly recorded in unambiguous oceanic crust adjacent to the Gascoyne Margin is chron M3n, which indicates full lithospheric rupture of the margin had occurred by ~130.6 Ma (Hauterivian; Figs 2B and 3A) (e.g., Robb et al. 2005; Direen et al. 2008).

Several tectonic elements are recognised within the Gascoyne Margin, including the Exmouth Plateau, and the Exmouth, Barrow, and Dampier sub-basins (Fig. 2A). The Exmouth Plateau comprises thin ($<$10 km thick) crystalline crust overlain by a $\leq$18 km-thick sedimentary sequence (e.g., Fig. 3B) (Pryer et al. 2002; Stagg et al. 2004). Sedimentary successions in the Exmouth and Barrow sub-basins are ~10–18 km thick (e.g., Fig. 3B), but locally up to ~24 km thick, making it difficult to seismically image the acoustic basement or Moho (e.g., Tindale et al. 1998). The lower portions of these sedimentary sequences are likely dominated by the Late Permian-to-Late Triassic, Locker Shale and Mungaroo Formation, which together are up to 9 km thick (Fig. 3) (e.g., Hocking et al. 1987; Stagg & Colwell 1994). The Exmouth Plateau was sediment-starved during Late Triassic-to-Jurassic rifting, preserving only a condensed ($\leq$100 m thick) stratigraphic record comprising clastic, shallow marine-to-deep marine, sedimentary strata of the Brigadier Formation, North Rankin Formation, Murat Siltstone, Athol Formation, and Dingo Claystone (e.g.,Hocking 1992; Boyd et al. 1993). Up to 4 km of Late Triassic-to-Jurassic strata accumulated in the Exmouth and Barrow sub-basins (Fig. 3) (e.g., Stagg & Colwell 1994). Tithonian-to-Valanginian rifting of the Gascoyne Margin provided accommodation for a $\leq$3.5 km thick sequence of clastic deltaic rocks of the Lower Barrow Group (Fig. 3) (e.g., Reeve et al. 2016; Paumard et al. 2018). A series of arches, which correspond to areas of localised uplift and erosion, occur across the Gascoyne Margin (Fig. 2) (e.g., Tindale et al. 1998): (i) the Alpha Arch likely formed in the Triassic-to-Jurassic in response to rift-related faulting and separates the Exmouth and Barrow Sub-basins; (ii) the Ningaloo Arch, erosion of which may have provided the source material for the Zeepaard Formation, is suggested to have formed during the Valanginian due to inversion driven by seafloor spreading in the Cuvier Abyssal Plain; and (iii) the Novara, Resolution, and Exmouth Plateau arches, which formed during post-breakup inversion events between the Santonian and present day.

2.1.2. Cuvier Margin

The 100–200 km wide Cuvier Margin has previously been interpreted to include a ~50 km wide COTZ, which borders the Cuvier Abyssal Plain to the NW (e.g., Fig. 2A) (Hopper et al. 1992; Colwell et al. 1994; Longley et al. 2002; Stagg et al. 2004). Proximal areas of the Cuvier Margin include the southern part of the Exmouth Sub-basin, which has been termed the Carnarvon Terrace (Fig. 2A) (e.g., Mihut & Müller 1998; Müller et al. 2002). The continental crust beneath the Carnarvon Terrace and South Carnarvon Basin is probably ~25–30 km thick (Hopper et al. 1992). Although the stratigraphy of the offshore Cuvier Margin is poorly constrained due to limited borehole data, it is likely similar to that of the northern Exmouth Sub-basin (Fig. 3A) (e.g., Partington et al. 2003; McClay et al. 2013). During Tithonian-to-Hauterivian rifting, uplift and erosion of the South Carnarvon Basin, perhaps driven by depth-dependent extension or dynamic topography, provided material for the Lower Barrow Group to the north (Reeve et al. 2016; Paumard et al. 2018).

Recognition of magnetic chrons M10N–M5n within assumed oceanic crust of the Cuvier Abyssal Plain has been used to suggest that breakup and lithospheric rupture of the

Cuvier Margin had occurred by ~136 Ma (Valanginian; Figs 2B and 3A) (Falvey & Veevers 1974; Larson et al. 1979); this model implies breakup of the Cuvier Margin occurred ~5 Myr before breakup of the Gascoyne Margin (Reeve et al. 2021). However, Reeve et al. (2021) recently recognised seaward-dipping reflector (SDR) sequences, which likely correspond to stacked lava flows, across the Cuvier Abyssal Plain. Based on sedimentological, biostratigraphic, and geochemical data, Reeve et al. (2021) infer these lava sequences were extruded within subaerial-to-shallow marine conditions and may have been contaminated by continental material. These constraints on lava emplacement and genesis suggest the Cuvier Abyssal Plain may actually be part of the Cuvier COTZ, as opposed to fully oceanic crust (Fig. 2) (Reeve et al. 2021). If the Cuvier Abyssal Plain is part of a COTZ, the oldest magnetic anomaly recorded in adjacent unambiguous oceanic crust (i.e. chron M3n) would imply full breakup of the Cuvier Margin occurred simultaneous to breakup along the Gascoyne Margin before ~130.6 Ma (Hauterivian) (Figs 2B and 3A) (e.g., Direen et al. 2008; Reeve et al. 2021).

2.2. Breakup-related unconformities and bounding strata

Three major unconformities are recognised in the North Carnarvon Basin that, based on their age, have been broadly related to continental breakup (Fig. 3) (e.g., Arditto 1993; Romine & Durrant 1996; Reeve et al. 2016): the Intra-Valanginian Unconformity (IVU); the Top Valanginian Unconformity (TVU); and the Intra-Hauterivian Unconformity (IHU).

2.2.1. Intra-Valanginian Unconformity

Previous terms for the IVU include the: Valanginian unconformity (e.g., Tindale et al. 1998; McClay et al. 2013); Intra-Valanginian sequence boundary (e.g., Romine & Durrant, 1996); KV seismic event or unconformity (e.g., Longley et al. 2002; Paumard et al. 2018); K-SAS5 sequence boundary (e.g., Jablonski 1997); K20.0 sequence boundary (e.g., Marshall & Lang 2013; Smith et al. 2015); Base Cretaceous unconformity (e.g., Baillie & Jacobson 1995; Müller et al. 2002); and breakup unconformity (e.g., Romine & Durrant 1996). The IVU commonly marks the top of the Lower Barrow Group and has been inferred to coincide with the boundary between the *Egmontodinium torynum* and *Systematophora areolata* dinoflagellate zones (Fig. 3A) (Arditto 1993; Labutis 1994; Smith et al. 2015; Paumard et al. 2018). This *E. torynum* and *S. areolata* dinoflagellate zone boundary was originally considered to occur at 138.2 Ma, which most studies adopt as the age of what we here refer to as the IVU (Fig. 3A) (e.g., Helby et al. 1987; Arditto 1993; Labutis 1994; Smith et al. 2015; Paumard et al. 2018). However, recent recalibration of these zones using biostratigraphic data from the North Scarborough-1 borehole suggests this boundary, and thus the IVU, could have formed later, between 137.55–134.98 Ma (Fig. 3A) (Gard et al. 2016).

Many studies relate the IVU to Early Cretaceous breakup of Australia and Greater India, and have linked the associated uplift driving its formation to: (i) a pre-breakup thermal event, perhaps related to the impingement of a mantle plume at the base of the crust (e.g., Rohrman 2015; Black et al. 2017), suggesting the IVU formed *before* lithospheric rupture and the onset of seafloor spreading (Fig. 3A); (ii) small-scale mantle convection driven by the juxtaposition of thin and thick lithosphere across the ~136 Myr old Cape Range Fracture Zone, suggesting the IVU formed *before* or *during* lithospheric rupture and the onset of seafloor spreading (e.g., Müller et al. 2002; Reeve et al. 2021); (iii) thermal uplift driven by the onset of oceanic crust formation to the north-west, suggesting the IVU formed *during* lithospheric rupture and seafloor spreading (cf. Fig. 3A) (e.g., Stagg & Colwell 1994; Romine & Durrant 1996); (iv) inversion and formation of the Ningaloo Arch, driven by ridge-push forces, suggesting the IVU formed *after* the onset of seafloor spreading (e.g., Tindale et al. 1998; Paumard et al. 2018); or (v) a major eustatic sea level fall and associated period of non-deposition, i.e. the formation of the IVU was not tectonically controlled (e.g., Jablonski 1997).

2.2.2. Top Valanginian Unconformity

The TVU has been interpreted to coincide with the boundary between the *S. areolata* and *Senoniasphaera tabulata* dinoflagellate zones (Fig. 3A) (Helby et al. 1987; Arditto 1993). This dinoflagellate zone boundary was originally considered to occur at 134.9 Ma, but recalibration of the North Scarborough-1 biostratigraphic data suggest it may be slightly younger (134.32–133.29 Ma; Figs 2B and 3A) (Gard et al. 2016). The TVU is locally recognised in the Exmouth and Barrow sub-basins and marks the top of the Zeepaard Formation, a relatively thin (<300 m thick), progradational deltaic sequence (Fig. 3A) (e.g., Arditto 1993; Paumard et al. 2018; Reeve et al. 2021). This unit has also been defined as the Upper Barrow Group (Paumard et al. 2018), but because it formed after the IVU in response to different uplift and subsidence processes relative to the Barrow Group *sensu stricto*, we refer to it as the Zeepaard Formation. The overlying, ~20–30 m thick Birdrong Sandstone Formation is sandstone-dominated, with minor siltstone and conglomerate, and was deposited in a shoreface environment (Thompson et al. 1990). The presence of the TVU between them suggests a period of minor uplift may have separated deposition of the Zeepard Formation and Birdrong Sandstone, although the processes driving this have not been considered.

2.2.3. Intra-Hauterivian Unconformity

The youngest breakup-related unconformity in the North Carnarvon Basin, the IHU, has been interpreted to coincide with the proposed ~132.5 Myr old boundary between the *Phoberocysta burgeri* and *Muderongia testudinaria* dinoflagellate zones (Fig. 3A) (Helby et al. 1987; Arditto 1993); the *P. burgeri* and *M. testudinaria* zones are missing or not sampled in the North Scarborough-1 borehole analysed by Gard et al. (2016). The IHU defines the top of the shallow marine Birdrong Sandstone, and the base of the overlying Mardie Greensand Member or Muderong Shale Formation (Fig. 3A) (e.g., Arditto 1993). The Mardie Greensand Member is predominantly composed of highly glauconitic sandstone, deposited in a shelfal marine environment; this unit passes laterally and vertically into the marine Muderong Shale Formation (Thompson et al. 1990).

3. Dataset and methodology

3.1. Data

We analyse a ~165,000 km^2 grid of publicly available 2D seismic data and twelve 3D reflection seismic datasets (Fig. 2B; see also Supplementary Table 2). Two-dimensional seismic line spacing ranges from ~0.5–10 km, but is typically <5 km. Vertical record length ranges from 3.5–16 s two-way travel-time (TWT). We use publicly available commercial palynology and micropalaeontology reports from 165 onshore and offshore boreholes to constrain stratigraphic ages above and below the breakup-related unconformities, and to investigate the abundance, timing, and distribution of sedimentary reworking related to margin uplift and erosion (Fig. 2B; see also Supplementary Table 3).

3.2. Unconformity mapping

We use checkshot data and borehole logs to tie well and seismic reflection data, allowing us to identify and map the IVU and IHU regionally within the 2D and 3D seismic reflection datasets. Where these unconformities were difficult to identify in seismic reflection data, or these data were unavailable, we use boreholes to constrain their stratigraphic context and extent. We do not regionally map the TVU within the seismic reflection data because its corresponding reflection is laterally discontinuous, making it difficult to confidently interpret; we instead define the position of the TVU using borehole data.

By using the mapped IVU and IHU horizons, we calculated the intervening stratal thickness of the Zeepaard Formation and Birdrong Sandstone to construct an isochore map. Because the Birdrong Sandstone is consistently 20–30 m thick (Thompson et al. 1990), we use this isochore map to identify major thickness changes in the substantially thicker Zeepaard Formation, allowing us to: (i) locate syn-depositional regions of relatively high and low accommodation, which we can potentially relate to areas of subsidence and uplift, respectively; and (ii) identify where uplift during development of the TVU or IHU may have led to the erosion of the Zeepaard Formation.

3.3. Calibration of dinoflagellate and calcareous nannofossil zones

Constraining the exact timing and duration of unconformity generation is often complicated by erosion of stratigraphy at the unconformable contact, which commonly represents a significant time gap (e.g., Miall 2016). Without confidence in age estimates for the unconformities, it is difficult to relate their formation to distinct tectonic and/or magmatic processes (e.g., Huang et al. 2017). The unconformities studied here have previously been correlated to dinoflagellate zone boundaries, but ages attributed to these palynological zonation schemes are poorly calibrated to the global chronostratigraphic timeframe (Fig. 3A) (e.g., Helby et al. 1987; Arditto 1993; Gard et al. 2016). To help constrain the age of unconformity formation we adopt a methodology similar to Gard et al. (2016), and use biostratigraphic data collected every 5 m from the Lightfinger-1 and Nimblefoot-1 boreholes to revise the timing of the *S. areolata* to *M. testudinaria* dinoflagellate zones. We use these boreholes because they intersect Early Cretaceous strata that preserves both dinoflagellate cysts *and* calcareous nannofossils, the global first and last occurrences of which are well-calibrated to the global chronostratigraphic timeframe (e.g., Gard et al. 2016). These well-calibrated calcareous nannofossil ages allow us to tie dinoflagellate zone boundaries to the global chronostratigraphy (Gard et al. 2016).

3.4. Unconformity subcrop and supercrop ages

We perform a joint analysis of seismic reflection and borehole data to constrain the ages of the sedimentary section directly above and below the breakup-related unconformities. Specifically, we use revised dinoflagellate zones to assign ages to the strata underlying (subcrop) and overlying (supercrop) the *oldest* breakup unconformity identifiable at each borehole location. For example, where all three breakup-related unconformities (i.e. IVU, TVU, and IHU) are present, we record the age of strata directly above and below the IVU. Where the IVU and TVU are eroded by the IHU, we record the age of strata directly above and below the IHU. Due to limitations in data availability, we focus on the oldest unconformities at each location because subcrop data for these allow us to reconstruct areas of relative uplift (or net-zero subsidence) and related erosion. Our interpreted palynology results for unconformity subcrop and supercrop ages at each well are included in Supplementary Table 2.

3.2.4. Reworking of palynomorphs

We investigate geographical changes in sediment source, which can help identify areas of uplift during IVU formation, by examining the reworking of early Valanginian (and earlier) palynomorphs in the Zeepaard Formation (see Reeve et al. 2016). For boreholes where reworking is not explicitly described in the palynology report, we utilise species occurrence charts, in addition to the stratigraphic age range for each species documented by Helby et al.

(1987), to assess whether older, reworked palynomorphs are present and, if so, their abundance.

4. Results

4.1. Distribution and structure of breakup-related unconformities

We recognise the IVU and IHU across most of the Gascoyne Margin, and note the IHU extends south onto the Cuvier Margin (Fig. 4). Across the northern sector of our study area the IVU is broadly a disconformity (purple colour in Fig. 4C), i.e. strata above and below are sub-parallel to its surface but there is an age gap between them (e.g., Figs 5A and B). In some places, underlying reflections are truncated by and overlying reflections onlap onto the IVU, particularly where it marks the arcuate, E-W trending clinoform front of the Lower Barrow Group (e.g., Figs 4A, 5A, and B). We also map a narrow (<50 km wide), E-trending zone along the southern extent of the IVU, across part of the Resolution Arch, where the truncation of underlying reflections is common; i.e. here the IVU becomes an angular unconformity (e.g., Figs 4C and 5C). Across these areas, the form of the TVU and IHU mirror the disconformable or angular nature of the underlying IVU (e.g., Figs 4C and 5A-C). In the south of the Exmouth Plateau, the IVU and IHU appear to merge (e.g., grey colour in Fig. 4C), but adjacent to the Cape Range Fracture Zone are themselves eroded by younger, post-breakup unconformities (green colour in Fig. 4C). Across the southern portion of the Exmouth Sub-basin, including over the Novara and Ningaloo arches, and Carnarvon Terrace the IHU defines a prominent angular unconformity, eroding into and forming a composite surface with the IVU and TVU (blue colour in Figs 4C and 5D).

4.2. Constraints on the age of Early Cretaceous unconformities

Here we describe the calcareous nannofossil and dinoflagellate occurrences within the strata bounding the breakup unconformities where they are intersected by the Lightfinger-1 and Nimblefoot-1 boreholes (Fig. 6). Using this information we later (section 5.1) recalibrate the ages of dinoflagellate zone boundaries that have previously been used to define the ages of the IVU, TVU, and IHU (e.g., Helby et al. 1987; Arditto 1993).

The lowermost calcareous nannofossils in Lightfinger-1 and Nimblefoot-1 that can help constrain the ages of the break-up unconformities are the first occurrences of *Eiffelithus striatus* (Fig. 6). In Lightfinger-1, *E. striatus* is first found at ~2655 m depth, within the *S. areolata* dinoflagellate zone and above the IVU, whereas in Nimblefoot-1 the first occurrence of *E. striatus* is found at ~2640 m depth within the *E. torynum* zone and below the IVU (Fig. 6). In Lightfinger-1, the last occurrence of *Eiffelithus windii* comprises a single palynomorph found at ~2610 m depth, above the IVU and immediately below the TVU (Fig. 6). Between the IVU and TVU in Nimblefoot-1, in the *S. areolata* dinoflagellate zone, the shallowest occurrences of *Cruciellipsis cuvillieri* (2630 m) and *Speetonia colligata* (2625 m) are found (Fig. 6).

There are no recorded samples from the *S. tabulata* dinoflagellate zone in either borehole (Fig. 6), which is expected to occur above the TVU (e.g., Helby et al. 1987; Arditto 1993). However, we note the first *Zeugrhabdotus scutula* and last *E. striatus* calcareous nannofossils are found directly above the TVU in Nimblefoot-1 at ~2615 m depth (Fig. 6). In contrast to Nimblefoot-1, there is an overlap between the occurrence of *Z. scutula* (~2560–2540 m depth) and the last occurrence of *E. striatus* (~2540 m depth), which was found alongside a single specimen of *Lithraphidites bolli*, within the *M. testudinaria* dinoflagellate zone above the IHU in Lightfinger-1 (Fig. 6). The shallowest samples from the *M.*

testudinaria dinoflagellate zone in Lightfinger-1 occur at ~2525–2530 m and also contain the shallowest occurrence of *C. cuvillieri* (Fig. 6).

4.3. Breakup-related sedimentary deposits

To investigate the distribution of uplift during and the sedimentary response to tectonic events during breakup, here we describe results from our analysis of the stratigraphic architecture and palynology of the Zeepaard Formation.

4.3.1. Unconformity subcrop

Tithonian-to-Valanginian strata of the Lower Barrow Group occur directly below the IVU, or the IHU where it has eroded the IVU; the exception to this is adjacent to the Australian coast where the subcropping rocks are Carboniferous-to-Upper Jurassic (Figs 3, 5A-C, and 7A). These subcropping Lower Barrow Group rocks typically belong to the *E. torynum* dinoflagellate zone, although in places over the Alpha Arch and particularly towards the coast they are of the older, *Batioladinium reticulatum* or *Dissimulidinium lobispinosum* dinoflagellate zones (Fig. 7A). Beneath the IHU, where it forms an angular unconformity, Lower Barrow Group rocks belonging to the *Pseudoceratium iehiense* dinoflagellate zone occur along an E-trending transect, across the Novara Arch (Fig. 7A). Further south, along the Cape Range Anticline and in two locations within the offshore Carnarvon Terrace, subcrop ages beneath the angular IHU range from Carboniferous-to-Upper Jurassic (Fig. 7A).

4.3.2. Unconformity supercrop strata

The Valanginian Zeepaard Formation, or its mudstone-dominated distal equivalent, typically overlies the IVU and corresponds to the *S. areolata* dinoflagellate zone (Figs 3, 5A-C, and 7B). Across parts of the Alpha Arch and particularly proximal to the Australian coast, the

IVU is overlain by the Birdrong Sandstone Formation (*S. tabulata*-to-*P. burgeri*) or Mardie Greensand (*S. tabulata*-to-*M. testudinaria*), comprising rocks that are younger than the Zeepaard Formation (Fig. 7B). The Birdrong Sandstone Formation and Mardie Greensand, as well as the Muderong Shale, also directly overlie the IHU where it has eroded the IVU and TVU (Fig. 7B). These supercropping rocks are typically attributable to the *M. australis* or *O. operculata* dinoflagellate zones (Fig. 7B).

4.3.3 Distribution and thickness of the Zeepaard Formation

The main depocentre of the Zeepaard Formation, where it is up to ~300 ms TWT thick, lies on the north-western flank of the Resolution Arch (Fig. 8A). From this main depocentre, the Zeepaard Formation thins westwards to ~25 ms TWT thick across its associated clinoform front, and eastwards to 75–150 ms in the Barrow Sub-basin (Fig. 8A). North of the Lower Barrow Group clinoform front, the distal equivalent of the Zeepaard Formation thickens to ~150–200 ms TWT (Fig. 8A). The Zeepaard Formation is absent across most of the Novara Arch and areas further south (Fig. 8A).

4.3.4. Palynology of the Zeepaard Formation

The Zeepaard Formation contains reworked Cretaceous, Jurassic, Triassic, and Permian palynomorphs (Fig. 8B). In some of its distal areas, adjacent to its clinoform front, the Zeepaard Formation contains only reworked Jurassic and Cretaceous palynomorphs (e.g., Spar-1, East Spar-1; Fig. 8B). North of its clinoform front, the Zeepaard Formation does not contain reworked palynomorphs (e.g., Mentorc-1, Satyr-1; Fig. 8B). Carboniferous or older reworking is scarce and only recorded in the York-1 and Woollybutt-3A boreholes (Fig. 8B). We do not observe evidence of palynomorph reworking in several wells on the Alpha Arch (i.e. Minden-1, Johnson-1, Bowers-1, and Nimrod-1; Fig. 8B).

5. Discussion

5.1. Timing of unconformity development and relationships to tectonic events

To help correlate unconformity development to discrete breakup-related events and processes, we recalibrate the local dinoflagellate palynomorph record that has previously been used to constrain the age of the IVU, TVU, and IHU (e.g., Helby et al. 1987; Arditto 1993). In particular, we tie palynomorph distribution to occurrences of calcareous nannofossils, which have globally robust age assignations (Gard et al. 2016). Here, we discuss how our recalibrated unconformity ages inform the breakup history of the Gascoyne and Cuvier margins.

5.1.1. IVU age and geodynamic significance

The IVU corresponds to the boundary between the *E. torynum–S. areolata* dinoflagellate zones, and has previously been interpreted to have formed in the Early Valanginian (138.2 Ma) *during* continental breakup and seafloor spreading (Fig. 3A) (e.g., Helby et al. 1987; Arditto 1993; Romine & Durrant 1996; Paumard et al. 2018). We show that strata below the IVU in Nimblefoot-1 contain *E. striatus* calcareous nannofossils (Fig. 6), which globally first appeared at 134.98 Ma and disappeared at 132.89 Ma (Gard et al. 2016); i.e. the IVU formed *after* 134.98 Ma. We note *E. striatus* nannofossils in Lightfinger-1 only occur *above* the IVU, in contrast to Nimblefoot-1 (Fig. 6), implying these do not record the global first occurrence of this species. The presence of these calcareous nannofossils indicate their host sedimentary rocks, located above and below the IVU, were deposited between 134.98–132.89 Ma (cf. Helby et al. 1987). Our borehole data also reveal the last occurrence of *E. windii* within Lightfinger-1 is ~60 m above the IVU, which indicates the unconformity formed, and at least part of the overlying Zeepaard Formation had been deposited, before the last global appearance of this calcareous nannofossil at 133.74 Ma (Fig. 6) (e.g., Gard et al. 2016). These distributions of *E. striatus* and *E. windii* calcareous nannofossils indicate the IVU formed in the Late Valanginian after 134.98 Ma and some time before 133.74 Ma, more recently than the previously proposed 138.2 Ma (Fig. 9) (cf. Helby et al. 1987). Formation of the IVU before 133.74 Ma is supported by the presence of *C. cuvillieri* and *Speetonia colligata* calcareous nannofossils, which globally last occurred at 132.88 Ma and 132.6 Ma respectively, between it and the TVU in Nimblefoot-1 (Fig. 6) (Reeve 2017). Development of the IVU between 134.98–133.74 Ma is also consistent with biostratigraphic constraints on its timing from the North Scarborough-1 borehole, supporting the recalibration of the *S. areolata* dinoflagellate zone as latest Valanginian-to-earliest Hauterivian (Fig. 9) (Gard et al. 2016).

A maximum age range of 134.98–133.74 Ma for IVU development indicates it formed synchronously to chrons M10N and M10 (135.9–133.6 Ma) within the Gascoyne Margin COTZ and Cuvier Abyssal Plain (Figs 2B, 9, and 10A) (e.g., Robb et al. 2005). If the Cuvier Abyssal Plain corresponds to a COTZ, similar to the Gascoyne Margin COTZ, the overlap in magnetic chron and IVU ages indicates uplift and unconformity development occurred *before* the breakup of both margins in the Hauterivian at ~131 Ma (Figs 9 and 10A) (e.g., Robb et al. 2005; Direen et al. 2008; Reeve et al. 2021). Conversely, if the Cuvier Abyssal Plain comprises ≲136 Myr old oceanic crust (e.g., Falvey & Veevers 1974; Larson et al. 1979; Hopper et al. 1992), an age range of 134.98–133.74 Ma for the IVU indicates it formed: (i) *after* continental breakup of the Cuvier Margin and *during* seafloor spreading; and (ii) *before* continental breakup of the Gascoyne Margin at ~131 Ma (Figs 9 and 10A). Regardless of the nature of the Cuvier Abyssal Plain, our age recalibration indicates the IVU did not coincide with continental breakup, i.e. full rupture of continental lithosphere (Figs 9 and 10A) (cf. Helby et al. 1987; Arditto 1993; Romine & Durrant 1996; Paumard et al. 2018).

5.1.2. TVU age and geodynamic significance

The TVU corresponds to the boundary between the *S. areolata*–*S. tabulata* dinoflagellate zones, and has previously been interpreted to have either formed in the Valanginian at 134.9 Ma (e.g., Helby et al. 1987; Arditto 1993) or between 134.32–133.29 Ma (Fig. 3A) (Gard et al. 2016). The recovery of *E. windii* immediately below the TVU in Lightfinger-1 suggests the unconformity could be younger than 133.74 Ma, but only if the presence of this calcareous nannofossil corresponds to its last global occurrence (Fig. 6) (e.g., Gard et al. 2016). Similarly, the presence of *C. cuvillieri* and *Speetonia colligata* calcareous nannofossils, below the TVU in Nimblefoot-1 suggests the unconformity could be younger 132.88–132.6 Ma, but only if these specimens correspond to their last global occurrence (Fig. 6) (Reeve 2017). However, we note the presence of *E. striatus*, which globally last appeared at 132.89 Ma (e.g., Gard et al. 2016), immediately above the TVU within Nimblefoot-1, indicating the unconformity is older than 132.89 Ma (Figs 3B, 7, and 10); i.e. the *C. cuvillieri* and *Speetonia colligata* calcareous nannofossils do not correspond to their last global occurrence. Constraining the onset and duration of TVU development further is difficult because there are no recognised occurrences of *S. tabulata* palynomorphs within Lightfinger-1 or Nimblefoot-1 (Fig. 7), which would be expected to occur in strata immediately above the unconformity (Figs 2A and 7) (e.g., Helby et al. 1987; Arditto 1993). This lack of *S. tabulata* occurrences may be because the strata hosting the palynomorphs are highly condensed at these borehole locations, so could have been missed by sampling at 5 m intervals. Previous studies from the Barrow Sub-basin have noted that the *S. tabulata* zone is highly facies dependent and therefore may not be recorded in the Exmouth Plateau due to palaeoenvironmental controls (e.g., Goodall 1999). Considering our recalibrated maximum age of the IVU is 134.98 Ma and given that the Zeepaard Formation was deposited between the IVU and TVU, our results indicate the TVU is younger than 134.98 Ma (Fig. 9) (cf. Helby et al. 1987). We thus suggest the TVU likely formed between ~134–133 Ma, dependent on when the IVU formed and how long it lasted, broadly consistent with dinoflagellate occurrences in the North Scarborough-1 borehole that suggest the *S. areolata*–*S. tabulata* zone boundary occurred at 133.29 Ma (Fig. 9) (Gard et al. 2016).

The potential formation of the TVU at ~134–133 Ma overlaps with chrons M10–M9 (~134.2–133 Ma; Figs 2B, 9, and 10A) (e.g., Robb et al. 2005). If the Cuvier Abyssal Plain corresponds to a COTZ, similar to the Gascoyne Margin COTZ, the overlap in ages of chrons M10, M9, and the TVU indicate uplift and unconformity development occurred *before* continental breakup of both margins in the Hauterivian at ~131 Ma (Figs 9 and 10A) (e.g., Robb et al. 2005; Direen et al. 2008). Conversely, if the Cuvier Abyssal Plain comprises $\lesssim$136 Myr old oceanic crust (e.g., Falvey & Veevers 1974; Larson et al. 1979; Hopper et al. 1992; Reeve et al. 2021), an age range of ~134–133 Ma for the TVU indicates it formed: (i) *after* continental breakup of the Cuvier Margin and *during* seafloor spreading; and (ii) *before* continental breakup of the Gascoyne Margin at ~131 Ma (Figs 9 and 10A).

5.1.3. IHU age and geodynamic significance

The IHU corresponds to the boundary between the *P. burgeri*–*M. testudinaria* dinoflagellate zones, and has previously been interpreted to have formed in the Hauterivian at ~132.5 Ma (Fig. 3A) (e.g., Helby et al. 1987; Mutterlose 1992). This inferred age of ~132.5 Ma is consistent with the coincidence between the first (~132.5 Ma) and last (132.89 Ma) occurrences of *Z. scutula* and *E. striatus*, respectively, in the *P.burgeri* dinoflagellate zone of Nimblefoot-1 ~30 m below the IHU (Fig. 7); these calcareous nannofossil occurrences suggest the IHU is younger than 132.5 Ma (Fig. 9). We note *E. striatus* and *C. cuvillieri* calcareous nannofossils are found *above* the IHU in Lightfinger-1, which both last appeared globally at ~132.9 Ma, and would imply the unconformity is older than the previously inferred age of 132.5 Ma (Fig. 7). However, we suggest these *E. striatus* and *C. cuvillieri* calcareous nannofossils have been reworked following erosion of older strata; i.e. the Lightfinger-1 data do not necessarily contradict an IHU age of $\lesssim$132.5 Ma. An age of 132.5 Ma for the IVU is also supported by the single specimen of *L. bolli*, which has a global range of 133.5–131. 5 Ma, in the *M. testudinaria* dinoflagellate zone of Lightfinger-1 above the IVU (Fig. 6) (Reeve 2017). Within the North Scarborough-1 borehole, Gard et al. (2016) dated an unnamed unconformity to 133.29–132.96 Ma, based on the last occurrence of *Crucibiscutum salebrosum* (132.96 Ma) above the last occurrence of *Stradnerlithus silvaradius* (133.29 Ma) in strata between depths of 1750–1760 m (Fig. 9) (Gard et al. 2016). We re-interpret the North Scarborough-1 palynological data and highlight that the ~133 Myr old strata intersected between depths of 1750–1760 m, which hosts the inferred unnamed unconformity, is overlain by rocks belonging to the *M. australis* dinoflagellate zone and are ~131–129 Ma (Hauterivian-to-Barremian) (Fig. 9) (Gard et al. 2016). We therefore interpret the unnamed unconformity in North Scarborough-1 is actually located above the last occurrence of *C. salebrosum* (132.96 Ma) in the *S. tabulata* dinoflagellate zone, immediately below the ~131–129 Ma *M. australis* dinoflagellate zone, and in fact is the IHU (cf. Gard et al. 2016). Where the IHU forms an angular unconformity across the southern Exmouth Sub-basin and Cuvier Margin, overlying strata also correspond to the *M. australis* dinoflagellate zone (Figs 5D and 7B). In summary, we suggest the IHU likely formed in the Hauterivian at some time between ~132.5–131 Ma (cf. Helby et al. 1987; Mutterlose 1992).

If our interpretation is correct, the formation of the IHU at ~132.5–131 Ma overlaps with chrons M7–M5n (~132.5–130.6 Ma; Figs 2B, 9, and 10A) (e.g., Robb et al. 2005). If the Cuvier Abyssal Plain corresponds to a COTZ, similar to the Gascoyne Margin COTZ, the overlap in ages of chrons M7–M5n and the IHU indicate uplift and unconformity development likely occurred immediately *before* or *during* continental breakup of both margins in the Hauterivian at ~131 Ma (Figs 9 and 10A) (e.g., Robb et al. 2005; Direen et al. 2008; Reeve et al. 2021). Conversely, if the Cuvier Abyssal Plain comprises $\lesssim$136 Myr old oceanic crust (e.g., Falvey & Veevers 1974; Larson et al. 1979; Hopper et al. 1992), an age range of ~132.5–131 Ma for the IHU indicates it formed: (i) *after* continental breakup of the Cuvier Margin and *during* seafloor spreading, broadly coincident with ridge jumps from the Sonne Ridge to the Sonja Ridge, and onto a spreading centre near Greater India (Robb et al. 2005); and (ii) immediately *before* or *during* continental breakup of the Gascoyne Margin at ~131 Ma (Figs 9 and 10A).

5.2. Uplift distribution during unconformity formation

Calibrating the timing of unconformity development is critical to interpreting how they relate temporally to continental breakup, but does not permit unambiguous constraint of the actual mechanisms driving their formation. Here, we discuss how the distribution of uplift, erosion, and non-deposition during IVU and IHU development spatially relates to the contemporaneous breakup events identified above (Fig. 10). Specifically, we use the seismic character of the unconformities, the age of sub- and supercropping strata, and the distribution of palynomorph reworking to map areas of uplift and erosion.

Across most of the Exmouth Plateau, northern Exmouth Sub-basin, and Barrow Sub-basin extent, the IVU and IHU appear as disconformities (Figs 4C and 5A-B); where the intervening TVU is recognised in seismic reflection data, its character mirrors that of the underlying IVU (e.g., Fig. 5C). Strata beneath the IVU, which corresponds to the Valanginian *E. torynum–S. areolata* dinoflagellate zone boundary, typically belong to the Lower Barrow Group and Valanginian *E. torynum*, or occasionally the Berriasian-to-Valanginian *B. reticulatum*, dinoflagellate zone (Fig. 7A). These occurrences of *E. torynum* and *B.*

reticulatum dinoflagellate zone subcrop ages indicate IVU development here involved little or no uplift and erosion; i.e. it marks a period of non-deposition. Strata above the IVU typically correspond to the Zeepaard Formation and Valanginian-to-Hauterivian *S. areolata* dinoflagellate zone, indicating the duration of unconformity formation was relatively short (Fig. 7B). Close to the Australian coast along the eastern portion of the Barrow Sub-basin and the Peedamullah Shelf, the IVU appears to overlie Permian-to-Jurassic strata and itself is overlain by rocks belonging to the Zeepaard Formation to Muderong Shale, particularly where it merges with older unconformities (Fig. 7). These variations in subcrop and supercrop ages of strata relative to the IVU in the Barrow Sub-basin and Peedamullah Shelf (Fig. 7) likely reflect the erosional and depositional history of such shallow marine settings, rather than the dynamics of unconformity formation.

Broadly southwards of the intersection between the Resolution and Novara arches, the IVU and IHU become angular unconformities (Figs 4C and 5C-D). For example, the IVU is recognised in seismic reflection data as an angular unconformity across an E-trending belt parallel to and >20 km north of the Ningaloo Arch (Figs 4C and 5C). Sparse well data in this area reveal IVU sub-crop ages range from Upper Jurassic to the Berriasian-to-Valanginian *B. reticulatum* dinoflagellate zone of the Lower Barrow Group, indicating the degree of erosion was spatially variable (Fig. 7A). South of this zone, the IHU, which likely corresponds to the Hauterivian *P. burgeri–M. testudinaria* dinoflagellate zone boundary, erodes into the Tithonian-to-Valanginian Lower Barrow Group over the Novara Arch and Triassic-to-Jurassic strata across the Carnarvon Terrace (Fig. 7A); from these data we thus cannot ascertain whether the underlying IVU originally extended further south (Fig. 10A). Strata above the IHU, where it corresponds to an angular unconformity, belong to the Hauterivian-to-Barremian *M. australis* or *O. operculata* dinoflagellate zones (Fig. 7B). These supercrop data indicate strata from the Hauterivian *M. testudinaria* dinoflagellate zone, which directly overlie the IHU to the north (e.g., in Lightfinger-1 and Nimblefoot-1), are missing across this southern area. Our seismic reflection mapping and analysis of sub- and supercrop ages suggests the onset of IHU formation occurred simultaneously across the study area, but only involved significant uplift and erosion south of the intersection between the Resolution and Novara arches; i.e. north of this area the IHU marks a period of non-deposition (Fig. 10B). We also show deposition onto the IHU resumed in the Hauterivian (*M. testudinaria* dinoflagellate zone) across most of the Exmouth Plateau, northern Exmouth Sub-basin, and Barrow Sub-basin, but to the south deposition resumed later in the Late Hauterivian-to-Barremian (*M. australis* dinoflagellate zone) (Fig. 7B). We cannot determine whether this diachroneity in the resumption of deposition indicates uplift and erosion in the southern half of our study area was maintained throughout the time gap represented by the IHU, or whether there was a lag between the end of uplift and the onset of deposition.

In addition to delimiting sub- and supercrop ages, high-resolution spatial and temporal constraints on uplift distribution are preserved in the provenance of reworked strata, if erosion of uplifted areas produces sedimentary deposits containing diagnostic compositional and microfossil assemblages (e.g., Reeve et al. 2016). The Zeepaard Formation clinoforms were deposited onto the IVU, prograded northwards, and were sourced from rocks hosting Early Cretaceous (Lower Barrow Group), Jurassic, Triassic, and Permian palynomorphs (Fig. 8). Compared to the underlying, pervasively reworked Lower Barrow Group, the degree of reworking in the Zeepaard Formation is less (e.g., Reeve et al. 2016), implying the two stratal units may have had different source areas; i.e. the formation of the IVU may have coincided with a change in regional uplift, erosion, and/or sediment dispersal patterns. Reeve et al. (2016) attributed prominent reworking of Permian and Triassic palynomorphs in the Lower Barrow Group to pre-breakup uplift of the South Carnarvon Basin. Based on the decrease in reworking abundance at the base of the Zeepaard Formation, we interpret that: (i) the rate of uplift of the South Carnarvon Basin, and thus erosion of Permian and Triassic strata, decreased during or immediately after IVU formation; and (ii) the Zeepaard Formation likely formed by recycling of Lower Cretaceous Lower Barrow Group, which contained previously reworked Jurassic–Permian palynomorphs (e.g., Reeve et al. 2016).

Overall, the localised angular character of the IVU, coupled with the areal coverage of and palynomorph distribution within the northwards-prograding Zeepaard Formation, suggests: (i) little or no uplift occurred across most of the Exmouth Plateau, northern Exmouth Sub-basin, and Barrow Sub-basin; (ii) uplift occurred at and south of the Novara Arch and southern half of the Resolution Arch; and (iii) erosion of the uplifted Lower Barrow Group and its correlative strata to the south provided material for the Zeepaard Formation (Fig. 10A). Our interpretation of uplift distribution during IVU development supports previous suggestions that formation and erosion of the Ningaloo Arch sourced the Zeepaard Formation (Fig. 10A) (Tindale et al. 1998). The Resolution and Novara arches have previously been linked to Santonian-to-Oligocene inversion (Tindale et al. 1998), but their apparent role in the formation of the IVU suggests they may have initially formed in the Valanginian and were later reactivated (Fig. 10A). The distribution of uplift, erosion, and non-deposition during IHU formation seems to mirror that of the IVU (Fig. 10B).

5.3. Possible mechanisms of breakup unconformity development

Breakup unconformities are typically considered to develop *during* continental breakup and the onset of seafloor spreading, in response to uplift driven by mantle upwelling, depth-dependent extension, and/or isostatic rebound (e.g., Falvey 1974; Cochran 1983; White & McKenzie 1988; Braun & Beaumont 1989; Issler et al. 1989; Morley 2016). Having calibrated the ages of unconformity development, which allow us to identify contemporaneous tectonic events, we can use our interpreted uplift distributions to explore possible mechanisms driving their formation (e.g., Gong et al. 2019).

Our recalibrated ages suggest the IVU (134.98–133.74 Ma) developed coincident to the generation of chrons M10N and M10 (135.9–133.6 Ma), during early formation of the Gascoyne Margin COTZ and the Cuvier Abyssal Plain (Figs 9 and 10A). Regardless of whether the Cuvier Abyssal Plain comprises oceanic crust or marks a COTZ (see Reeve et al. 2021 and references therein), our results indicate the IVU coincided with: (i) the localisation of extension along narrow continental rift zones (Gascoyne and possibly Cuvier margin), which can become COTZs (e.g., as inferred by Bridges et al. 2012 in the onshore Gulf of Aden rift, Ethiopia), and perhaps a seafloor spreading centre within the Cuvier Abyssal Plain; and (ii) an increase in magmatism focused along the axis of extension, which produced the igneous rocks that carry the magnetic chron signature (e.g., as inferred by Collier et al. 2017 along the South Atlantic rifted margin). Similar migration (from inboard to outboard positions) and localisation of extension through time has been recognised from both active rifts and ancient rifted margins, where such narrow zones of extension play an important role in the late-stages of rifting and transition to seafloor spreading (e.g., Ebinger & Casey 2001; Geoffroy 2005; Corti 2009; Bastow & Keir 2011; Bastow et al. 2018; Peron-Pinvidic et al. 2019; Pérez-Gussinyé et al. 2020).

The presence of seaward-dipping reflector (SDR) lava sequences observed across chrons M10N and M10 in both the Gascoyne Margin COTZ and Cuvier Abyssal Plain (Direen et al. 2008; Reeve et al. 2021), indicates that as crust moved away from the elevated extension axis it subsided and created space for SDR emplacement (Fig. 10C) (e.g., Corti et al. 2015; Buck 2017; Paton et al. 2017). Our analysis shows uplift and erosion was focused along the continental Cuvier Margin during the subsidence and drift of the Gascoyne Margin COTZ and Cuvier Abyssal Plain from the extension axis (Fig. 10A); we lack sufficient data to determine whether uplift also occurred along the distal Gascoyne Margin adjacent to its COTZ (Fig. 10A). We thus suggest unconformity development likely reflects localised rift flank uplift (Pérez-Gussinyé et al. 2020), perhaps driven by depth-dependent extension following strain localisation along rift zones in the Gascoyne Margin COTZ and Cuvier Abyssal Plain; i.e. lower crustal and/or lithospheric material flowed landward away from rift axis and subsiding COTZ to under the rift flanks (Fig. 10C) (e.g., Huismans & Beaumont 2011). Such transient depth-dependent extension could have: (i) been instigated by intrusion-induced heating of the crust (Daniels et al. 2014); and (ii) produced the observed uplift patterns recorded by and captured in the distribution of the IVU, by inducing margin-wide uplift and unconformity development, peaking along the Exmouth Plateau, Exmouth Sub-basin, and Carnarvon Terrace areas (e.g., the Novara Arch). Models involving depth-dependent extension have previously been proposed to explain the architecture and subsidence history of the Gascoyne Margin (Stagg & Colwell 1994; Driscoll & Karner 1998; Frey et al. 1998; Stagg et al. 2004; Huismans & Beaumont 2011; Reeve et al. 2016). Small-scale mantle convection generated at the boundary between the thicker Gascoyne lithosphere and the thinner Cuvier lithosphere may also have contributed to uplift of the Cuvier Margin (e.g., Müller et al. 2002).

Our recalibrated age of ~134–133 Ma for the TVU suggests it formed during the COTZ development of the Gascoyne Margin, and seafloor spreading or COTZ development of the Cuvier Abyssal Plain (Fig. 9). We lack constraints on uplift distribution during the time at which the TVU formed, but we suggest its development may have been related to the generation of new magmatic crust along sub-aerial, or perhaps shallow-marine, spreading ridges in the COTZ(s) (Collier et al. 2017; Paton et al. 2017; McDermott et al. 2018).

Our recalibrated ages suggest the IHU (~132.5–131 Ma) probably developed simultaneously to the formation of chrons M7–M5n (~132.5–130.6 Ma), likely coinciding with the onset of full continental lithosphere rupture along the Gascoyne Margin, and perhaps the Cuvier Margin (Figs 2B, 9, and 10A). The IHU therefore seems to best fit the classic interpretation of a breakup unconformity as forming at the onset of seafloor spreading (e.g., Falvey 1974; Soares et al. 2012). We note that the distribution of disconformable and angular portions of the IHU broadly mirror those of the IVU, suggesting uplift was again focused along the rift flanks within the continental margins in response to depth-dependent extension (Fig. 10C).

Overall, our work supports previous findings that continental breakup processes are variable in time and space, and can involve multiple episodes of uplift and unconformity development (e.g., Soares et al. 2012; Alves & Cunha 2018; Gong et al. 2019; Monteleone et al. 2019; Xie et al. 2019). We also demonstrate that migration of rift axes probably plays an important role in controlling the occurrence, distribution, and magnitude of breakup unconformities (Pérez-Gussinyé et al. 2020). Stratigraphic successions on continental rifted margins provide a critical record of these complex breakup processes, but unlocking these archives can be difficult and requires integrating geological and geophysical analyses (e.g., Soares et al. 2012; Gong et al. 2019; Monteleone et al. 2019; Peron-Pinvidic et al. 2019; Pérez-Gussinyé et al. 2020).

6. Conclusions

Breakup unconformities are common features observed along rifted margins and are typically assumed to occur at the onset of seafloor spreading, perhaps in response to uplift driven by asthenospheric upwelling, isostatic rebound, and or depth-dependent extension. Using an integrated geological and geophysical approach, we present a regional-scale interpretation of the stratigraphic expression of continental breakup in the North Carnarvon Basin, offshore NW Australia, and its implications for margin evolution. During the breakup of the Gascoyne and Cuvier margins NW Australia, three unconformities developed over ~4 Myr, rather than a single ‘breakup unconformity’ *sensu stricto.* Our recalibration of high-resolution biostratigraphic data constrain the timing of these unconformities and allows us to relate their genesis to the tectonic record preserved in the magnetic stripes of adjacent continent-ocean transition zones (COTZs) and oceanic crust. We find that: (i) the Intra-Valanginian Unconformity developed between 134.98–133.74 Ma, not at 138.2 Ma as previously suggested, broadly coincident with localisation of strain to magma-rich, narrow rift zones during continent-ocean transition, and possibly seafloor spreading; (ii) the Top Valanginian Unconformity, which likely formed at ~134–133 Ma, perhaps in response to sub-aerial magmatic spreading within COTZs; and (iii) the Intra-Hauterivian Unconformity probably formed between at ~132.5–131 Ma during the onset of full lithospheric rupture of the Gascoyne, and perhaps Cuvier, margins. By mapping unconformity subcrop and supercrop ages, coupled with examining thickness variations and palynomorph reworking within the inter-unconformity Zeepaard Formation, we demonstrate uplift and erosion was focused along the continental Cuvier Margin, adjacent to its COTZ. The unconformities across most of the Gascoyne Margin are disconformable and likely reflect non-deposition rather than uplift and erosion. We speculate that localisation of uplift occurred along the rift flanks due to periodic depth-dependent extension during COTZ, and perhaps oceanic crust, formation. Our work shows that the ‘breakup unconformity’ is not necessarily a single, simple stratigraphic surface related to the onset of oceanic crust formation, but may instead be represented by multiple unconformities reflecting a complex history of uplift and subsidence during the transition from continental rifting to seafloor spreading.

Acknowledgements

We thank Schlumberger for provision of Petrel licenses to Imperial College London. Geoscience Australia and the Department of Mines and Petroleum are thanked for provision of data. M.T.R. was supported by NERC grant NE/L501621/L. Gwenn Peron-Pinvidic, Gareth Roberts, and Saskia Goes are thanked for helpful discussions during the preparation of this manuscript.

Data Availability

Seismic reflection and well data used in this study are available from the WAPIMS (https://wapims.dmp.wa.gov.au/wapims/) and NOPIMS (https://www.nopims.gov.au/) data repositories.

Figure captions

Figure 1: Map showing global distribution of breakup unconformity locations from previous studies. Topography and bathymetry are from ETOPO1 Global Relief Model (Amante & Eakins 2009). For details of references used for each breakup unconformity location, see Supplementary Table 1.

Figure 2: (A) Map of the North and South Carnarvon basins highlighting principal tectonic elements, including: ExP = Exmouth Plateau, ExSB = Exmouth Sub-basin, CT = Carnarvon Terrace, BSB = Barrow Sub-basin, DSB = Dampier Sub-basin, PS = Peedamullah Shelf, PB = Perth Basin, WS = Wallaby Saddle, WP = Wallaby Plateau, CAP = Cuvier Abyssal Plain, GAP = Gascoyne Abyssal Plain, SR = Sonne Ridge, SjR = Sonja Ridge, CRFZ = Cape Range Fracture Zone, WZFZ = Wallaby-Zenith Fracture Zone. The location of the Resolution Arch (*RA*), Exmouth Plateau Arch (*EA*), Alpha Arch (*AA*), Novara Arch (*NA*),

and Ningaloo Arch (*NiA*) are also shown. Elevation data are based on the 2009 Australian Bathymetry and Topography grid (Geoscience Australia). Inset: Location map of the North Carnarvon Basin (NCB) relative to Australia and the Gascoyne and Cuvier margins. (B) Map showing extent of 2D and 3D seismic reflection data coverage and locations of boreholes used in this study. Total magnetic intensity grid (EMAG2v2) also shown with interpreted magnetic chrons (based on Robb et al. 2005). See Supplementary Figure S1 for an uninterpreted version.

Figure 3: (A) Stratigraphic column for the Exmouth Plateau, Exmouth Sub-basin and Cuvier Margin summarising the age, dominant lithology, and generalised depositional environment for key units (after Hocking et al. 1987; Hocking 1992; Arditto 1993; Partington et al. 2003). Dinoflagellate zone schemes from Helby et al. (1987) and Gard et al. (2016) highlighting their implications for unconformity timing; grey areas encompass the possible age of respective dinoflagellate zone boundaries. Numerical ages and geomagnetic polarity also shown (Gradstein et al. 2012; Cohen et al. 2013; updated). Key tectonics events shown for comparison; two scenarios for the Cuvier Abyssal Plain (CAP) are included where it is either oceanic crust of a continent-ocean transition zone (COTZ) (see Reeve et al. 2021 and references therein). (B) Uninterpreted and interpreted seismic section, showing generalised stratigraphic architecture of the Exmouth Plateau and Exmouth Sub-basin. See Figure 2B for location and Figure 3A for key.

Figure 4: (A) Two-way time structure map of the Intra-Valanginian Unconformity (IVU) seismic horizon. (B) Two-way time structure map of the Intra-Hauterivian Unconformity (IHU) seismic horizon. (C) Map showing the interpreted structural configuration of the Intra-Valanginian and Intra-Hauterivian unconformities.

Figure 5: (A) Uninterpreted and interpreted zoomed-in seismic section focusing on the IVU and IHU Figure 3B. See Figure 3B for key. (B) Uninterpreted and interpreted seismic section from the southern Exmouth Plateau, showing the relationship of the IVU and IHU to the Lower Barrow Group and overlying stratigraphy. See Figure 4 for location and Figure 3B for key. (B) Uninterpreted and interpreted seismic section from the Novara Arch area, showing the relationship between Early Cretaceous unconformities and breakup-related compressional structures See Figure 4 for location and Figure 3B for key. (D) Uninterpreted and interpreted seismic section from the Carnarvon Terrace showing the structural style of the Intra-Hauterivian Unconformity and underlying stratigraphy. See Figure 4 for location and Figure 3B for key.

Figure 6: Recorded dinoflagellate zones, gamma ray logs and key calcareous nannofossil first/last occurrences in the Lightfinger-1 and Nimblefoot-1 wells. Depth values are measured depth with respect to well rotary table. Inset: Location map of boreholes within the Glencoe 3D survey (see Fig. 2B for survey location).

Figure 7: (A) Map showing the youngest recorded stratigraphic ages beneath the breakup unconformity (subcrop) in wells from the onshore and offshore North and South Carnarvon Basins, based on palynology reports. The location of the Resolution Arch (*RA*), Exmouth Plateau Arch (*EA*), Alpha Arch (*AA*), Novara Arch (*NA*), and Ningaloo Arch (*NiA*) are also shown. (B) Map showing the oldest recorded dinoflagellate zones and formation above the breakup unconformity (supercrop) in wells from the onshore and offshore North and South Carnarvon Basins, based on palynology reports.

Figure 8: (A) Vertical two-way time thickness map of the Zeepaard and Birdrong Formations based on seismic interpretation. (B) Map showing well locations from the Exmouth Plateau and Exmouth and Barrow Sub-basins where Early Cretaceous, Jurassic, Triassic, Permian and Carboniferous age palynomorphs are recorded within the Zeepaard Formation.

Figure 9: Comparison of previously published dinoflagellate zone ages of Helby et al. (1987) and Gard et al. (2016) to our recalibrated dinoflagellate zone ages. In the North Scarborough-1 borehole, Gard et al. (2016) defined an unnamed unconformity (?), which we interpret as being the IHU. Numerical ages and magnetic polarity chrons (Gradstein et al. 2012; Cohen et al. 2013; updated), in addition to generalised tectono-magmatic evolution of the Gascoyne and Cuvier Abyssal Plains also shown; two scenarios for the Cuvier Abyssal Plain (CAP) are included where it is either oceanic crust of a continent-ocean transition zone (COTZ) (see Reeve et al. 2021 and references therein).

Figure 10: (A and B) Schematic palaeogeographic reconstructions showing the development of the IVU and IHU, and areas of associated uplift, with respect to formation of the Gascoyne Margin COTZ and the Cuvier Abyssal Plain (after Reeve et al. 2021). (C) Schematic section showing how magma-dominated extension along a rift axis or spreading centre could promote lower crustal and/or lithospheric mantle to flow and accumulate beneath the continental margin rift flank, causing it to uplift. SDRs = seaward-dipping reflectors. Possible line locations shown in (A).

10. References

Alves, T.M. & Cunha, T.A. 2018. A phase of transient subsidence, sediment bypass and deposition of regressive–transgressive cycles during the breakup of Iberia and Newfoundland. *Earth and Planetary Science Letters*, **484**, 168-183.

Amante, C. & Eakins, B.W. 2009. *ETOPO1 arc-minute global relief model: procedures, data sources and analysis.* National Oceanic and Atmospheric Administration.

Arditto, P.A. 1993. Depositional sequence model for the post-Barrow Group Neocomian succession, Barrow and Exmouth sub-basins, Western Australia. *The APPEA Journal*, **33**, 151-160.

Baillie, P. & Jacobson, E. 1995. Structural evolution of the Carnarvon Terrace, Western Australia. *The APPEA Journal*, **35**, 321-332.

Bastow, I.D. & Keir, D. 2011. The protracted development of the continent-ocean transition in Afar. *Nature Geoscience*, **4**, 248-250.

Bastow, I.D., Booth, A.D., Corti, G., Keir, D., Magee, C., Jackson, C.A.L., Warren, J., Wilkinson, J.*, et al.* 2018. The Development of Late-Stage Continental Breakup: Seismic Reflection and Borehole Evidence from the Danakil Depression, Ethiopia. *Tectonics*, **37**, 2848-2862.

Black, M., McCormack, K., Elders, C. & Robertson, D. 2017. Extensional fault evolution within the Exmouth Sub-basin, North West Shelf, Australia. *Marine and petroleum geology*, **85**, 301-315.

Bott, M.H. 1982. The mechanism of continental splitting. *Tectonophysics*, **81**, 301-309.

Boyd, R., Williamson, P. & Haq, B. 1993. Seismic stratigraphy and passive-margin evolution of the southern Exmouth plateau. *In*: Posamentier, H., Summerhayes, C., Haq, B. & Allen, G. (eds) *Sequence stratigraphy and facies associations*. Blackwell Publishing Ltd, 579-603.

Braun, J. & Beaumont, C. 1989. A physical explanation of the relation between flank uplifts and the breakup unconformity at rifted continental margins. *Geology*, **17**, 760-764.

Bridges, D.L., Mickus, K., Gao, S.S., Abdelsalam, M.G. & Alemu, A. 2012. Magnetic stripes of a transitional continental rift in Afar. *Geology*, **40**, 203-206.

Buck, W.R. 2017. The role of magmatic loads and rift jumps in generating seaward dipping reflectors on volcanic rifted margins. *Earth and Planetary Science Letters*, **466**, 62-69.

Cande, S.C. & Mutter, J.C. 1982. A revised identification of the oldest sea-floor spreading anomalies between Australia and Antarctica. *Earth and Planetary Science Letters*, **58**, 151-160.

Cochran, J.R. 1983. Effects of finite rifting times on the development of sedimentary basins. *Earth and Planetary Science Letters*, **66**, 289-302.

Cohen, K.M., Finney, S.C., Gibbard, P.L. & Fan, J.-X. 2013; updated. The ICS international chronostratigraphic chart. *Episodes*, **36**, 199-204.

Collier, J.S., McDermott, C., Warner, G., Gyori, N., Schnabel, M., McDermott, K. & Horn, B.W. 2017. New constraints on the age and style of continental breakup in the South Atlantic from magnetic anomaly data. *Earth and Planetary Science Letters*, **477**, 27-40.

Colwell, J., Symonds, P. & Crawford, A. 1994. The nature of the Wallaby (Cuvier) Plateau and other igneous provines of the west Australian margin. *Journal of Australian Geology and Geophysics*, **15**, 137-156.

Corti, G. 2009. Continental rift evolution: from rift initiation to incipient break-up in the Main Ethiopian Rift, East Africa. *Earth-Science Reviews*, **96**, 1-53.

Corti, G., Agostini, A., Keir, D., Van Wijk, J., Bastow, I.D. & Ranalli, G. 2015. Magma-induced axial subsidence during final-stage rifting: Implications for the development of seaward-dipping reflectors. *Geosphere*, **11**, 563-571.

Dafoe, L.T., Keen, C.E., Dickie, K. & Williams, G.L. 2017. Regional stratigraphy and subsidence of Orphan Basin near the time of breakup and implications for rifting processes. *Basin Research*, **29**, 233-254.

Daniels, K.A., Bastow, I.D., Keir, D., Sparks, R.S.J. & Menand, T. 2014. Thermal models of dyke intrusion during development of continent–ocean transition. *Earth and Planetary Science Letters*, **385**, 145-153, http://doi.org/http://dx.doi.org/10.1016/j.epsl.2013.09.018.

Direen, N.G., Stagg, H.M.J., Symonds, P.A. & Colwell, J.B. 2008. Architecture of volcanic rifted margins: new insights from the Exmouth – Gascoyne margin, Western Australia. *Australian Journal of Earth Sciences*, **55**, 341-363, http://doi.org/10.1080/08120090701769472.

Driscoll, N.W. & Karner, G.D. 1998. Lower crustal extension across the Northern Carnarvon basin, Australia: Evidence for an eastward dipping detachment. *Journal of Geophysical Research: Solid Earth (1978–2012)*, **103**, 4975-4991.

Driscoll, N.W., Hogg, J.R., Christie-Blick, N. & Karner, G.D. 1995. Extensional tectonics in the Jeanne d'Arc Basin, offshore Newfoundland: implications for the timing of break-up between Grand Banks and Iberia. *Geological Society, London, Special Publications*, **90**, 1-28.

Ebinger, C.J. & Casey, M. 2001. Continental breakup in magmatic provinces: An Ethiopian example. *Geology*, **29**, 527-530, http://doi.org/10.1130/0091-7613(2001)029<0527:cbimpa>2.0.co;2.

Embry, A.F. & Dixon, J. 1990. The breakup unconformity of the Amerasia Basin, Arctic Ocean: evidence from arctic Canada. *Geological Society of America Bulletin*, **102**, 1526-1534.

Falvey, D. & Veevers, J. 1974. Physiography of the Exmouth and Scott plateaus, western Australia, and adjacent northeast Wharton Basin. *Marine Geology*, **17**, 21-59.

Falvey, D.A. 1974. The development of continental margins in plate tectonic theory. *The APPEA Journal*, **14**, 95-106.

Franke, D. 2013. Rifting, lithosphere breakup and volcanism: Comparison of magma-poor and volcanic rifted margins. *Marine and petroleum geology*, **43**, 63-87.

Frey, Ø., Planke, S., Symonds, P.A. & Heeremans, M. 1998. Deep crustal structure and rheology of the Gascoyne volcanic margin, western Australia. *Marine Geophysical Researches*, **20**, 293-311.

Gard, G., Backhouse, J. & Crux, J. 2016. Calibration of Early Cretaceous dinoflagellate zones from the NWS of Australia to the global time scale through calcareous nannofossils. *Cretaceous Research*, **61**, 180-187.

Geoffroy, L. 2005. Volcanic passive margins. *Comptes Rendus Geoscience*, **337**, 1395-1408, http://doi.org/10.1016/j.crte.2005.10.006.

Gillard, M., Autin, J., Manatschal, G., Sauter, D., Munschy, M. & Schaming, M. 2015. Tectonomagmatic evolution of the final stages of rifting along the deep conjugate Australian-Antarctic magma-poor rifted margins: Constraints from seismic observations. *Tectonics*, **34**, 753-783.

Gong, Y., Lin, C., Zhang, Z., Zhang, B., Shu, L., Feng, X., Hong, F., Xing, Z., *et al.* 2019. Breakup unconformities at the end of the early Oligocene in the Pearl River Mouth Basin, South China Sea: significance for the evolution of basin dynamics and tectonic geography during rift–drift transition. *Marine Geophysical Research*, **40**, 371-384.

Goodall, J. 1999. *Palynological Review of East Spar and Spar-1*.

Gradstein, F.M., Ogg, J.G., Schmitz, M.B. & Ogg, G.M. 2012. *The geologic time scale 2012*. Elsevier.

Heine, C. & Müller, R. 2005. Late Jurassic rifting along the Australian North West Shelf: margin geometry and spreading ridge configuration. *Australian Journal of Earth Sciences*, **52**, 27-39.

Helby, R., Morgan, R. & Partridge, A. 1987. A palynological zonation of the Australian Mesozoic. *Memoir of the Association of Australasian Palaeontologists*, **4**, 1-94.

Hocking, R. 1992. Jurassic deposition in the southern and central North West Shelf. *Western Australia: Geological Survey Western Australia Record*, **199217**.

Hocking, R.M., Moors, H.T. & Van de Graaff, W.E. 1987. *Geology of the carnarvon basin, Western Australia*. State Print. Division.

Hopper, J.R., Mutter, J.C., Larson, R.L. & Mutter, C.Z. 1992. Magmatism and rift margin evolution: Evidence from northwest Australia. *Geology*, **20**, 853-857.

Huang, C.-Y., Shea, K.-H. & Li, Q. 2017. A foraminiferal study on Middle Eocene-Oligocene break-up unconformity in northern Taiwan and its correlation with IODP Site U1435 to constrain the onset event of South China Sea opening. *Journal of Asian Earth Sciences*, **138**, 439-465.

Huismans, R. & Beaumont, C. 2011. Depth-dependent extension, two-stage breakup and cratonic underplating at rifted margins. *Nature*, **473**, 74-78.

Issler, D., McQueen, H. & Beaumont, C. 1989. Thermal and isostatic consequences of simple shear extension of the continental lithosphere. *Earth and Planetary Science Letters*, **91**, 341-358.

Jablonski, D. 1997. Recent advances in the sequence stratigraphy of the Triassic to Lower Cretaceous succession in the Northern Carnarvon Basin, Australia. *The APPEA Journal*, **37**, 429-454.

Labutis, V. 1994. Sequence stratigraphy and the North West Shelf of Australia. *In*: Purcell, P. & PUrcell, R. (eds.) *The Sedimentary Basins of Western Australia: Proceedings of the Petroleum Exploration Society of Australia Symposium*, 159-180.

Larsen, H. & Saunders, A. 1998. 41. Tectonism and volcanism at the Southeast Greenland rifted margin: a record of plume impact and later continental rupture. *Proceedings of the Ocean Drilling Program, Scientific Results*, 503-533.

Larson, R.L., Mutter, J.C., Diebold, J.B., Carpenter, G.B. & Symonds, P. 1979. Cuvier Basin: a product of ocean crust formation by Early Cretaceous rifting off Western Australia. *Earth and Planetary Science Letters*, **45**, 105-114.

Lavin, C. 1997. The Maastrichtian Breakup of the Otway Basin Margin–a Model Developed by Integrating Seismic Interpretation, Sequence Statigraphy and Thermochronological Studies. *Exploration Geophysics*, **28**, 252-259.

Le Pichon, X. & Sibuet, J.C. 1981. Passive margins: a model of formation. *Journal of Geophysical Research: Solid Earth*, **86**, 3708-3720.

Longley, I., Buessenschuett, C., Clydsdale, L., Cubitt, C., Davis, R., Johnson, M., Marshall, N., Murray, A., *et al.* 2002. The North West Shelf of Australia–a Woodside perspective. *The sedimentary basins of Western Australia*, **3**, 27-88.

Marshall, N. & Lang, S. 2013. A new sequence stratigraphic framework for the North West Shelf, Australia. *The Sedimentary Basins of Western Australia 4: Proceedings PESA Symposium. Perth*, 1-32.

McClay, K., Scarselli, N. & Jitmahantakul, S. 2013. Igneous intrusions in the Carnarvon Basin, NW Shelf, Australia. *In*: Keep, M. & Moss, S.J. (eds) *The Sedimentary Basins of Western Australia IV*. Proceedings of the Petroleum Exploration Society of Australia Symposium, Perth, WA.

McDermott, C., Lonergan, L., Collier, J.S., McDermott, K.G. & Bellingham, P. 2018. Characterization of Seaward-Dipping Reflectors Along the South American Atlantic Margin and Implications for Continental Breakup. *Tectonics*, **37**, 3303-3327.

McKenzie, D. 1978. Some remarks on the development of sedimentary basins. *Earth and Planetary Science Letters*, **40**, 25-32.

Menzies, M., Klemperer, S., Ebinger, C. & Baker, J. 2002. Characteristics of volcanic rifted margins. *In*: Menzies, M., Klemperer, S., Ebinger, C. & Baker, J. (eds) *Volcanic Rifted Margins, Special Publications*. Geological Society of America, **362**, 1-14.

Miall, A.D. 2016. The valuation of unconformities. *Earth-Science Reviews*, **163**, 22-71.

Mihut, D. & Müller, R.D. 1998. Volcanic margin formation and Mesozoic rift propagators in the Cuvier Abyssal Plain off Western Australia. *Journal of Geophysical Research*, **103**, 27135-27127,27149.

Mohriak, W.U. & Leroy, S. 2013. Architecture of rifted continental margins and break-up evolution: insights from the South Atlantic, North Atlantic and Red Sea–Gulf of Aden conjugate margins. *Geological Society, London, Special Publications*, **369**, 497-535.

Monteleone, V., Minshull, T.A. & Marin-Moreno, H. 2019. Spatial and temporal evolution of rifting and continental breakup in the Eastern Black Sea Basin revealed by long-offset seismic reflection data. *Tectonics*, **38**, 2646-2667.

Morley, C. 2016. Major unconformities/termination of extension events and associated surfaces in the South China Seas: Review and implications for tectonic development. *Journal of Asian Earth Sciences*, **120**, 62-86.

Müller, R., Mihut, D., Heine, C., O’Neill, C. & Russell, I. 2002. Tectonic and volcanic history of the Carnarvon Terrace: Constraints from seismic interpretation and geodynamic modelling. *The sedimentary basins of Western Australia*, **3**, 719-740.

Mutterlose, J. 1992. Biostratigraphy and palaeobiogeography of Early Cretaceous calcareous nannofossils. *Cretaceous Research*, **13**, 167-189.

Partington, M., Aurisch, K., Clark, W., Newlands, I., Phelps, S., Senycia, P., Siffleet, P. & Walker, T. 2003. The hydrocarbon potential of exploration permits WA-299-P and WA-300-P, Carnarvon Basin: a case study. *The APPEA Journal*, **43**, 339-361.

Paton, D., Pindell, J., McDermott, K., Bellingham, P. & Horn, B. 2017. Evolution of seaward-dipping reflectors at the onset of oceanic crust formation at volcanic passive margins: Insights from the South Atlantic. *Geology*, **45**, 439-442.

Paumard, V., Bourget, J., Payenberg, T., Ainsworth, R.B., George, A.D., Lang, S., Posamentier, H.W. & Peyrot, D. 2018. Controls on shelf-margin architecture and sediment partitioning during a syn-rift to post-rift transition: Insights from the Barrow Group (Northern Carnarvon Basin, North West Shelf, Australia). *Earth-Science Reviews*, **177**, 643-677.

Pérez-Gussinyé, M., Andrés-Martínez, M., Araújo, M., Xin, Y., Armitage, J. & Morgan, J. 2020. Lithospheric Strength and Rift Migration Controls on Synrift Stratigraphy and Breakup Unconformities at Rifted Margins: Examples From Numerical Models, the Atlantic and South China Sea Margins. *Tectonics*, **39**, e2020TC006255.

Peron-Pinvidic, G., Manatschal, G. & Participants, a.t.I.R.W. 2019. Rifted margins: state of the art and future challenges. *Frontiers in Earth Science*, **7**, 8.

Pryer, L., Romine, K., Loutit, T. & Barnes, R. 2002. Carnarvon basin architecture and structure defined by the integration of mineral and petroleum exploration tools and techniques. *The APPEA Journal*, **42**, 287-309.

Reeve, M.T. 2017. *The structural and stratigraphic expression of continental breakup.* Imperial College London.

Reeve, M.T., Jackson, C.A.L., Bell, R.E., Magee, C. & Bastow, I.D. 2016. The stratigraphic record of prebreakup geodynamics: Evidence from the Barrow Delta, offshore Northwest Australia. *Tectonics*, **35**, 1935-1968.

Reeve, M.T., Magee, C., Bastow, I.D., McDermott, C., Jackson, C.A.-L., Bell, R.E. & Prytulak, J. 2021. Nature of the Cuvier Abyssal Plain crust, offshore NW Australia. *Journal of the Geological Society*.

Robb, M.S., Taylor, B. & Goodliffe, A.M. 2005. Re-examination of the magnetic lineations of the Gascoyne and Cuvier Abyssal Plains, off NW Australia. *Geophysical Journal International*, **163**, 42-55.

Rohrman, M. 2015. Delineating the Exmouth mantle plume (NW Australia) from denudation and magmatic addition estimates. *Lithosphere*, L445. 441.

Romine, K. & Durrant, J. 1996. *Carnarvon Cretaceous-Tertiary Tie Report.* Australian Geological Society Organisation.

Skogseid, J., Pedersen, T., Eldholm, O. & Larsen, B.T. 1992. Tectonism and magmatism during NE Atlantic continental break-up: the Voring Margin. *Geological Society, London, Special Publications*, **68**, 305-320, http://doi.org/10.1144/gsl.sp.1992.068.01.19.

Smith, T., Ogg, J., Kelman, A., Abbott, S. & Bernecker, T. 2015. Towards common stratigraphic frameworks for Australia's offshore hydrocarbon provinces. *The APPEA Journal*, **2015**, 105-112.

Soares, D.M., Alves, T.M. & Terrinha, P. 2012. The breakup sequence and associated lithospheric breakup surface: Their significance in the context of rifted continental margins (West Iberia and Newfoundland margins, North Atlantic). *Earth and Planetary Science Letters*, **355**, 311-326.

Stagg, H. & Colwell, J. 1994. The structural foundations of the Northern Carnarvon Basin. *The sedimentary basins of Western Australia: Proceedings of Petroleum Exploration Society of Australia Symposium, Perth*, 349-365.

Stagg, H., Alcock, M., Bernardel, G., Moore, A., Symonds, P. & Exon, N. 2004. *Geological framework of the outer Exmouth Plateau and adjacent ocean basins*. Geoscience Australia.

Symonds, P.A., Planke, S., Frey, O. & Skogseid, J. 1998. Volcanic evolution of the Western Australian Continental Margin and its implications for basin development. *The Sedimentary Basins of Western Australia 2: Proc. of Petroleum Society Australia Symposium, Perth, WA*.

Thompson, N., Hocking, R., Collins, M., Voon, J. & Middleton, M. 1990. *Lower Cretaceous deposition in the southern Northwest Shelf.* Minerals and Energy Research Institute of Western Australia.

Tindale, K., Newell, N., Keall, J. & Smith, N. 1998. Structural evolution and charge history of the Exmouth Sub-basin, northern Carnarvon Basin, Western Australia. *The Sedimentary Basins of Western Australia 2: Proc. of Petroleum Society Australia Symposium, Perth, WA*, 473-490.

Tucholke, B., Sawyer, D. & Sibuet, J.-C. 2007. Breakup of the Newfoundland–Iberia rift. *Geological Society, London, Special Publications*, **282**, 9-46.

Veevers, J. 1986. Breakup of Australia and Antarctica estimated as mid-Cretaceous (95±5 Ma) from magnetic and seismic data at the continental margin. *Earth and Planetary Science Letters*, **77**, 91-99.

White, N. & McKenzie, D. 1988. Formation of the" steer's head" geometry of sedimentary basins by differential stretching of the crust and mantle. *Geology*, **16**, 250-253.

Willcox, J. & Exon, N.J.T.A.J. 1976. The regional geology of the Exmouth Plateau. **16**, 1-11.

Xie, X., Ren, J., Pang, X., Lei, C. & Chen, H. 2019. Stratigraphic architectures and associated unconformities of Pearl River Mouth basin during rifting and lithospheric breakup of the South China Sea. *Marine Geophysical Research*, **40**, 129-144.

Figure 1

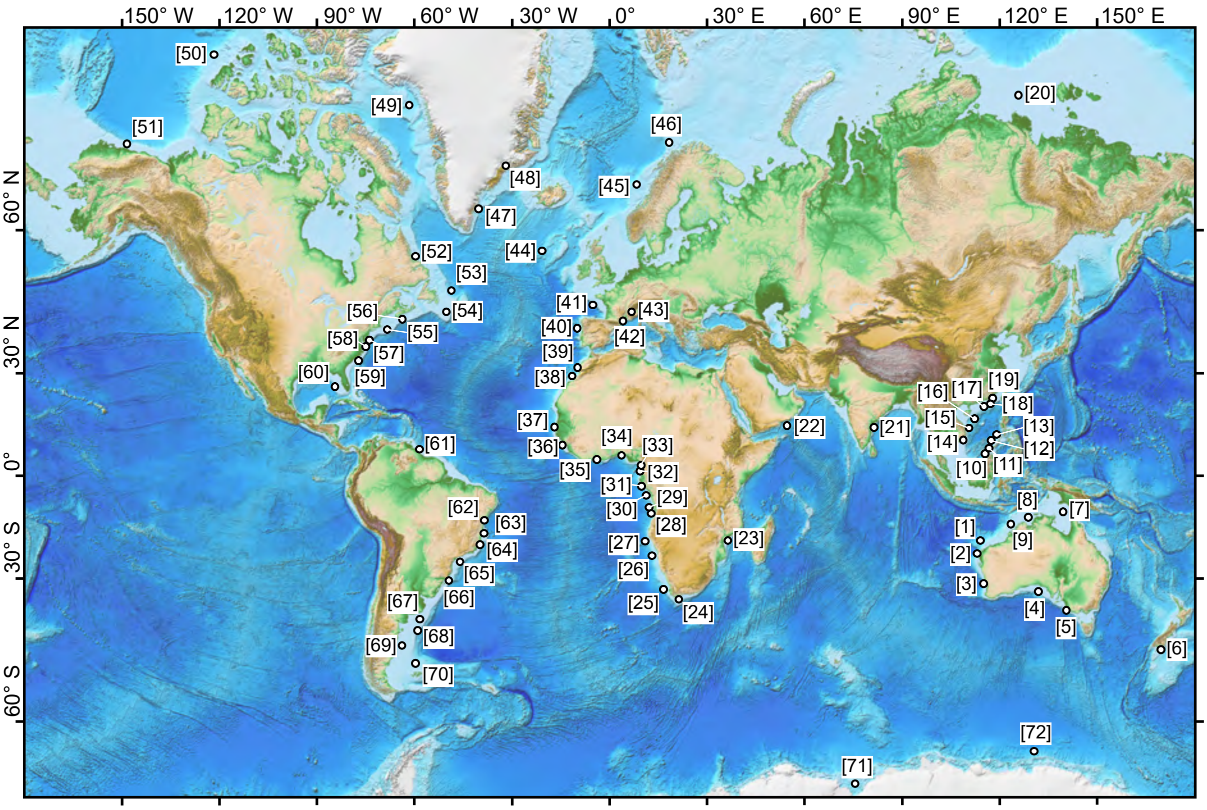
150° W
120° W
90° W
60° W
30° W
0°
30° E
60° E
90° E
120° E
150° E
60° N
30° N
0°
30° S
60° S
[1]
[2]
[3]
[4]
[5]
[6]
[7]
[8]
[9]
[10]
[11]
[12]
[13]
[14]
[15]
[16]
[17]
[18]
[19]
[20]
[21]
[22]
[23]
[24]
[25]
[26]
[27]
[28]
[29]
[30]
[31]
[32]
[33]
[34]
[35]
[36]
[37]
[38]
[39]
[40]
[41]
[42]
[43]
[44]
[45]
[46]
[47]
[48]
[49]
[50]
[51]
[52]
[53]
[54]
[55]
[56]
[57]
[58]
[59]
[60]
[61]
[62]
[63]
[64]
[65]
[66]
[67]
[68]
[69]
[70]
[71]
[72]

Figure 2

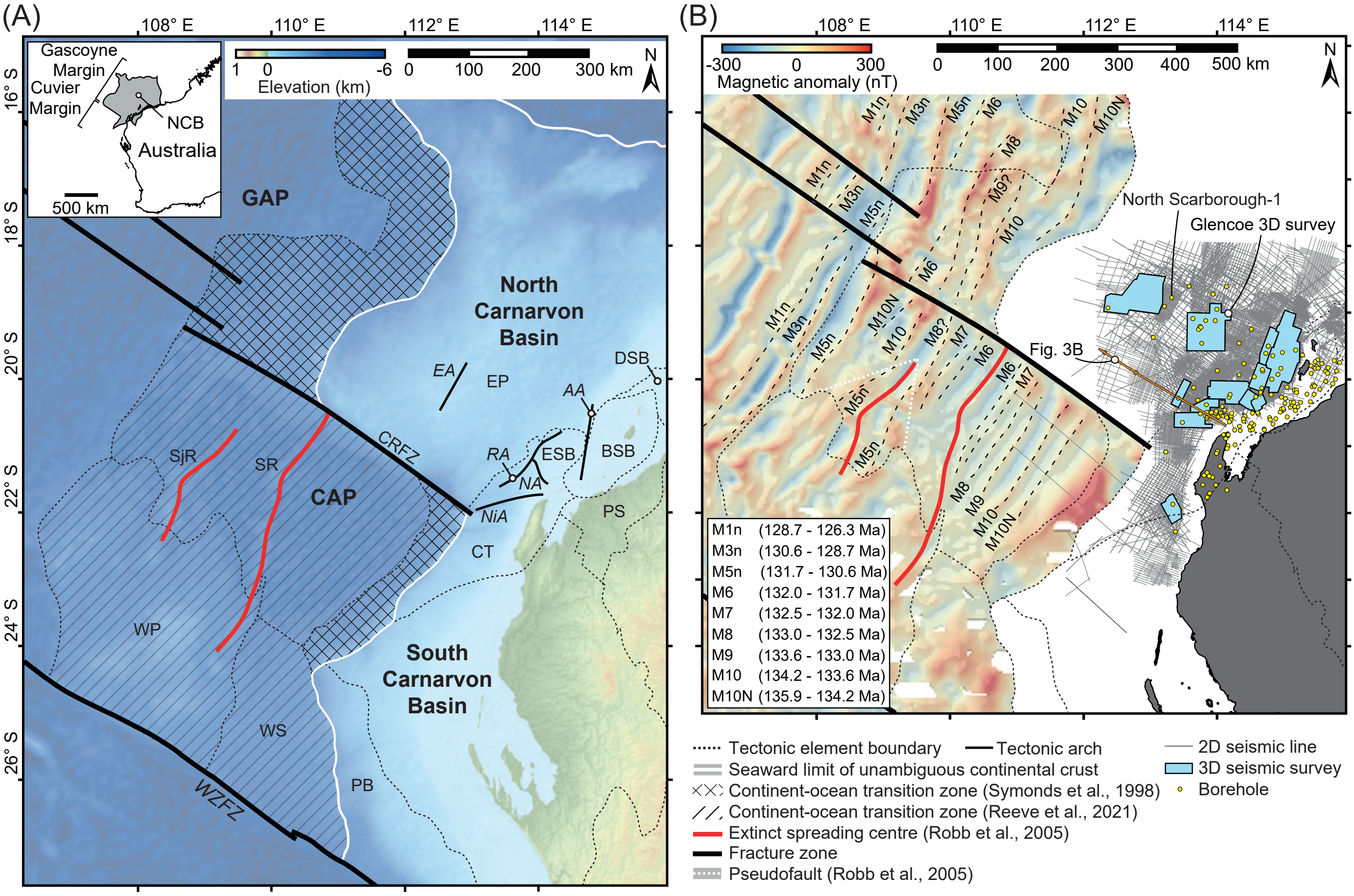

(A)
(B)
108° E
110° E
112° E
114° E
16° S
18° S
20° S
22° S
24° S
26° S
Gascoyne Margin
Cuvier Margin
NCB
Australia
500 km
1 0 -6
Elevation (km)
0 100 200 300 km
N
GAP
North Carnarvon Basin
EA
EP
AA
DSB
RA
ESB
BSB
NA
NiA
CRFZ
SjR
SR
CAP
PS
CT
WP
South Carnarvon Basin
WS
WZFZ
PB
-300 0 300
Magnetic anomaly (nT)
0 100 200 300 400 500 km
North Scarborough-1
Glencoe 3D survey
Fig. 3B
M1n (128.7 - 126.3 Ma)
M3n (130.6 - 128.7 Ma)
M5n (131.7 - 130.6 Ma)
M6 (132.0 - 131.7 Ma)
M7 (132.5 - 132.0 Ma)
M8 (133.0 - 132.5 Ma)
M9 (133.6 - 133.0 Ma)
M10 (134.2 - 133.6 Ma)
M10N (135.9 - 134.2 Ma)
Tectonic element boundary
Tectonic arch
2D seismic line
Seaward limit of unambiguous continental crust
3D seismic survey
Continent-ocean transition zone (Symonds et al., 1998)
Borehole
Continent-ocean transition zone (Reeve et al., 2021)
Extinct spreading centre (Robb et al., 2005)
Fracture zone
Pseudofault (Robb et al., 2005)

Figure 3

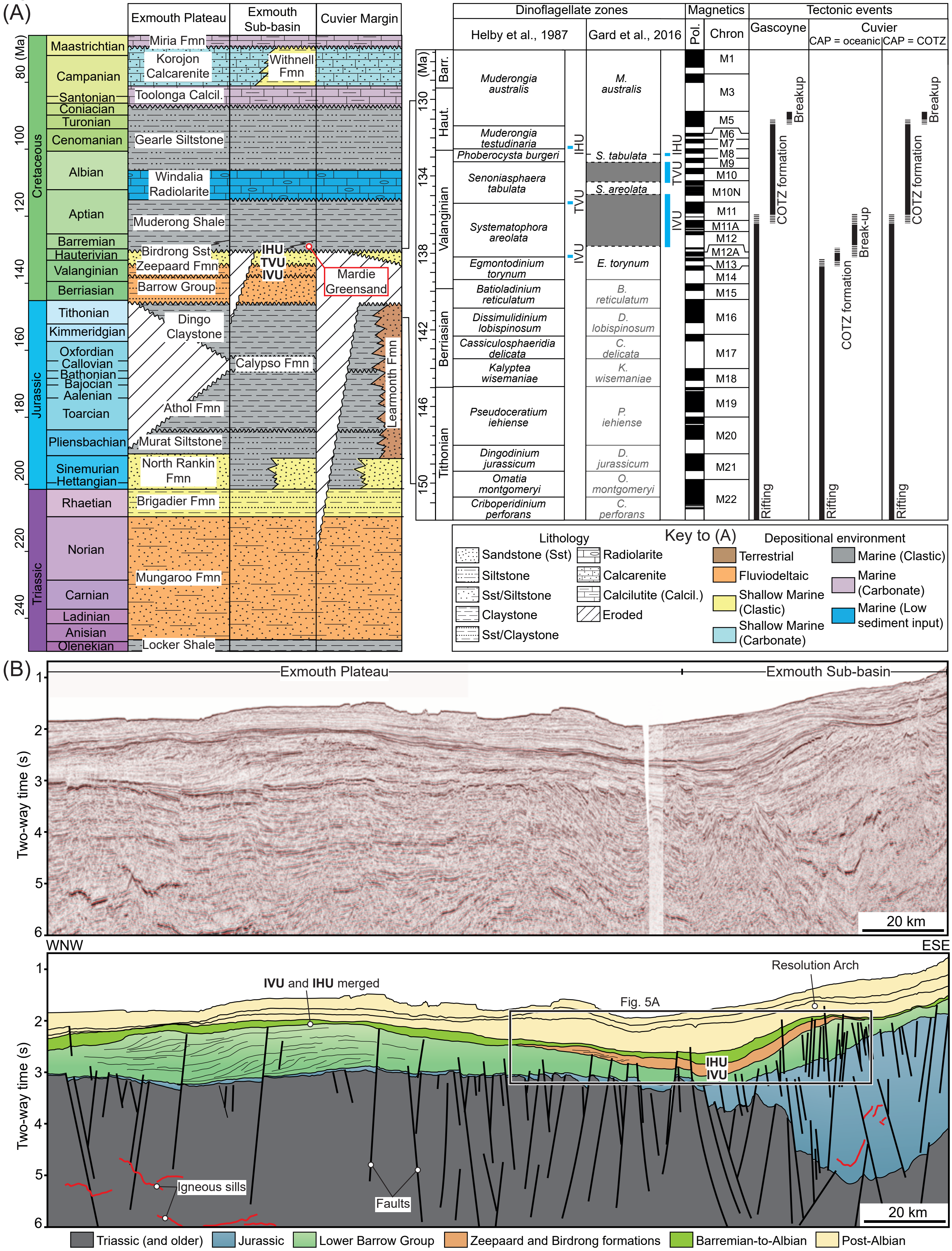
(A)
Exmouth Plateau
Exmouth Sub-basin
Cuvier Margin
Maastrichtian
Campanian
Santonian
Coniacian
Turonian
Cenomanian
Albian
Aptian
Barremian
Hauterivian
Valanginian
Berriasian
Tithonian
Kimmeridgian
Oxfordian
Callovian
Bathonian
Bajocian
Aalenian
Toarcian
Pliensbachian
Sinemurian
Hettangian
Rhaetian
Norian
Carnian
Ladinian
Anisian
Olenekian
Cretaceous
Jurassic
Triassic
(Ma)
Miria Fmn
Korojon Calcarenite
Withnell Fmn
Toolonga Calcil.
Gearle Siltstone
Windalia Radiolarite
Muderong Shale
Birdrong Sst
Zeepaard Fmn
Barrow Group
IHU
TVU
IVU
Mardie Greensand
Dingo Claystone
Calypso Fmn
Athol Fmn
Learmonth Fmn
Murat Siltstone
North Rankin Fmn
Brigadier Fmn
Mungaroo Fmn
Locker Shale
Dinoflagellate zones
Helby et al., 1987
Gard et al., 2016
Magnetics
Pol.
Chron
Tectonic events
Gascoyne
Cuvier
CAP = oceanic
CAP = COTZ
Barr.
Haut.
Valanginian
Berriasian
Tithonian
Muderongia australis
Muderongia testudinaria
Phoberocysta burgeri
Senoniasphaera tabulata
Systematophora areolata
Egmontodinium torynum
Batioladinium reticulatum
Dissimulidinium lobispinosum
Cassiculosphaeridia delicata
Kalyptea wisemaniae
Pseudoceratium iehiense
Dingodinium jurassicum
Omatia montgomeryi
Cribroperidinium perforans
M. australis
S. tabulata
S. areolata
E. torynum
B. reticulatum
D. lobispinosum
C. delicata
K. wisemaniae
P. iehiense
D. jurassicum
O. montgomeryi
C. perforans
M1
M3
M5
M6
M7
M8
M9
M10
M10N
M11
M11A
M12
M12A
M13
M14
M15
M16
M17
M18
M19
M20
M21
M22
Rifting
COTZ formation
Breakup
Break-up
Key to (A)
Lithology
Sandstone (Sst)
Siltstone
Sst/Siltstone
Claystone
Sst/Claystone
Radiolarite
Calcarenite
Calcilutite (Calcil.)
Eroded
Depositional environment
Terrestrial
Fluviodeltaic
Shallow Marine (Clastic)
Shallow Marine (Carbonate)
Marine (Clastic)
Marine (Carbonate)
Marine (Low sediment input)
(B)
Exmouth Plateau
Exmouth Sub-basin
Two-way time (s)
20 km
WNW
ESE
IVU and IHU merged
Fig. 5A
Resolution Arch
IHU
IVU
Igneous sills
Faults
Triassic (and older)
Jurassic
Lower Barrow Group
Zeepaard and Birdrong formations
Barremian-to-Albian
Post-Albian

Figure 4

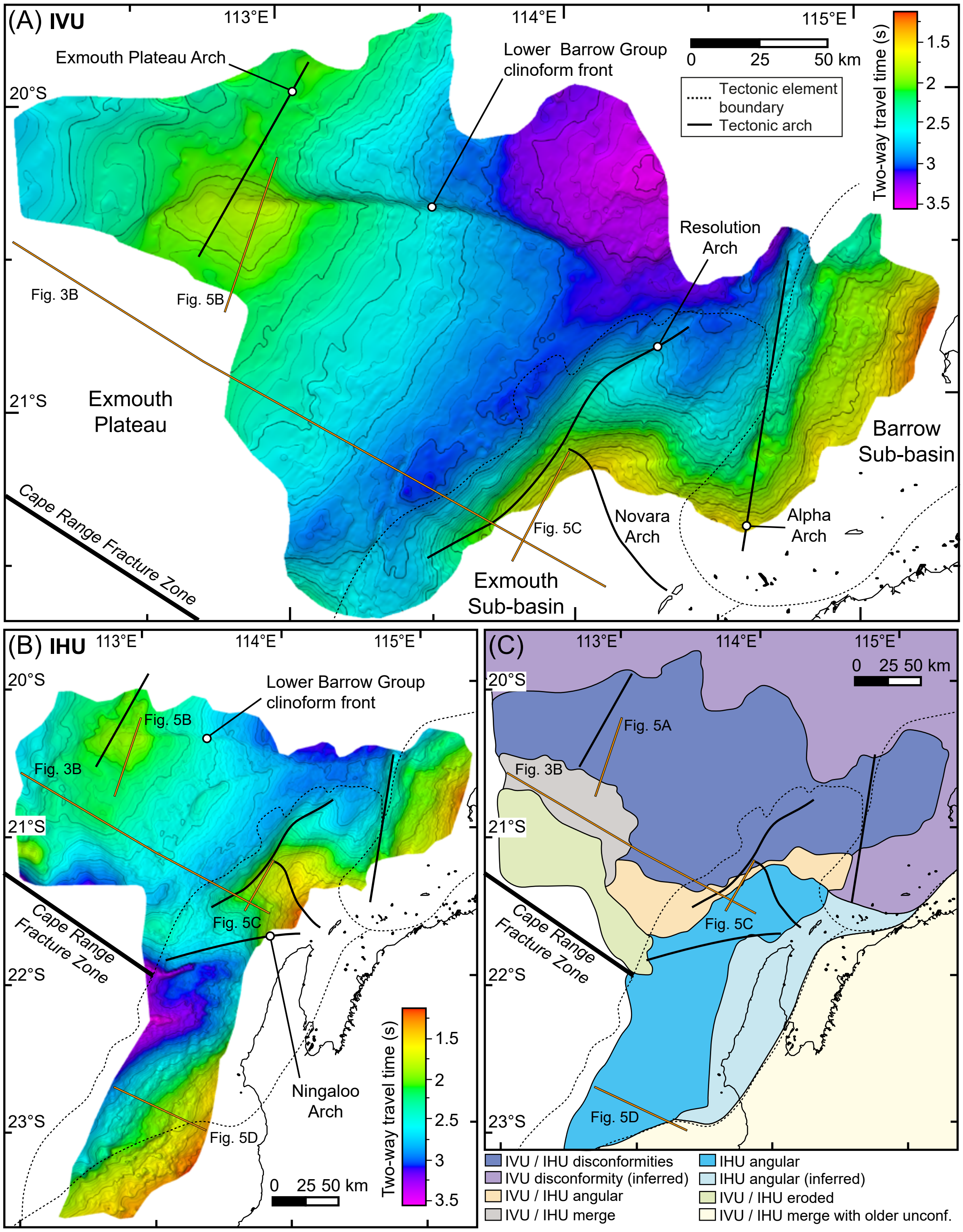

(A) IVU
113°E
114°E
115°E
Exmouth Plateau Arch
Lower Barrow Group
clinoform front
0 25 50 km
Tectonic element boundary
Tectonic arch
Two-way travel time (s)
1.5
2
2.5
3
3.5
20°S
21°S
Resolution Arch
Fig. 3B
Fig. 5B
Exmouth Plateau
Barrow Sub-basin
Novara Arch
Alpha Arch
Fig. 5C
Exmouth Sub-basin
Cape Range Fracture Zone
(B) IHU
113°E
114°E
115°E
20°S
21°S
22°S
23°S
Lower Barrow Group
clinoform front
Fig. 5B
Fig. 3B
Fig. 5C
Cape Range Fracture Zone
Ningaloo Arch
Fig. 5D
Two-way travel time (s)
1.5
2
2.5
3
3.5
0 25 50 km
(C)
113°E
114°E
115°E
0 25 50 km
20°S
21°S
22°S
23°S
Fig. 5A
Fig. 3B
Fig. 5C
Cape Range Fracture Zone
Fig. 5D
IVU / IHU disconformities
IVU disconformity (inferred)
IVU / IHU angular
IVU / IHU merge
IHU angular
IHU angular (inferred)
IVU / IHU eroded
IVU / IHU merge with older unconf.

Figure 5

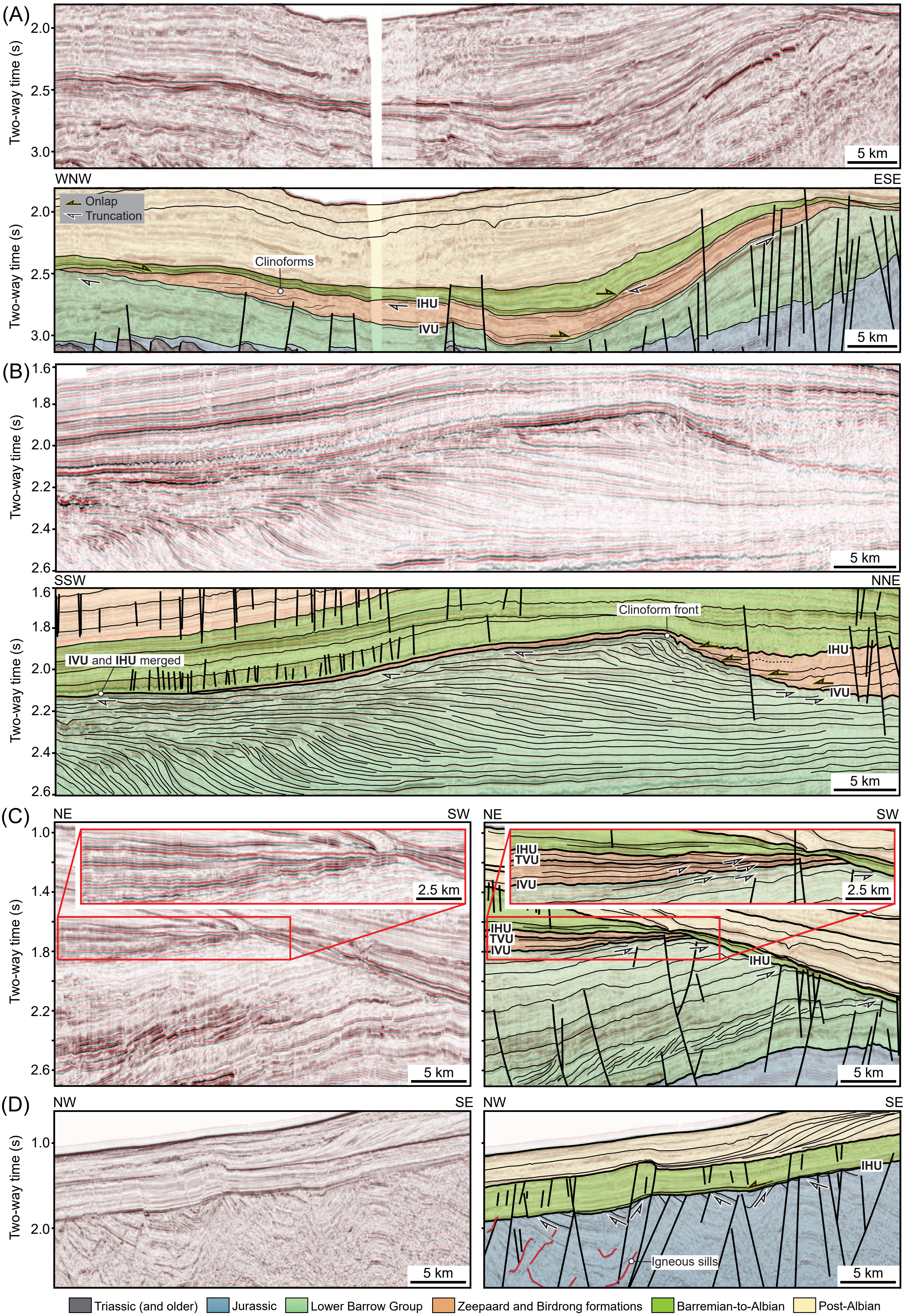

(A)
Two-way time (s)
2.0
2.5
3.0
5 km
WNW
ESE
Onlap
Truncation
Clinoforms
IHU
IVU
(B)
1.6
1.8
2.0
2.2
2.4
2.6
SSW
NNE
Clinoform front
IVU and IHU merged
IHU
IVU
(C)
NE
SW
1.0
1.4
1.8
2.2
2.6
2.5 km
IHU
TVU
IVU
(D)
NW
SE
Igneous sills
Triassic (and older)
Jurassic
Lower Barrow Group
Zeepaard and Birdrong formations
Barremian-to-Albian
Post-Albian

Figure 6

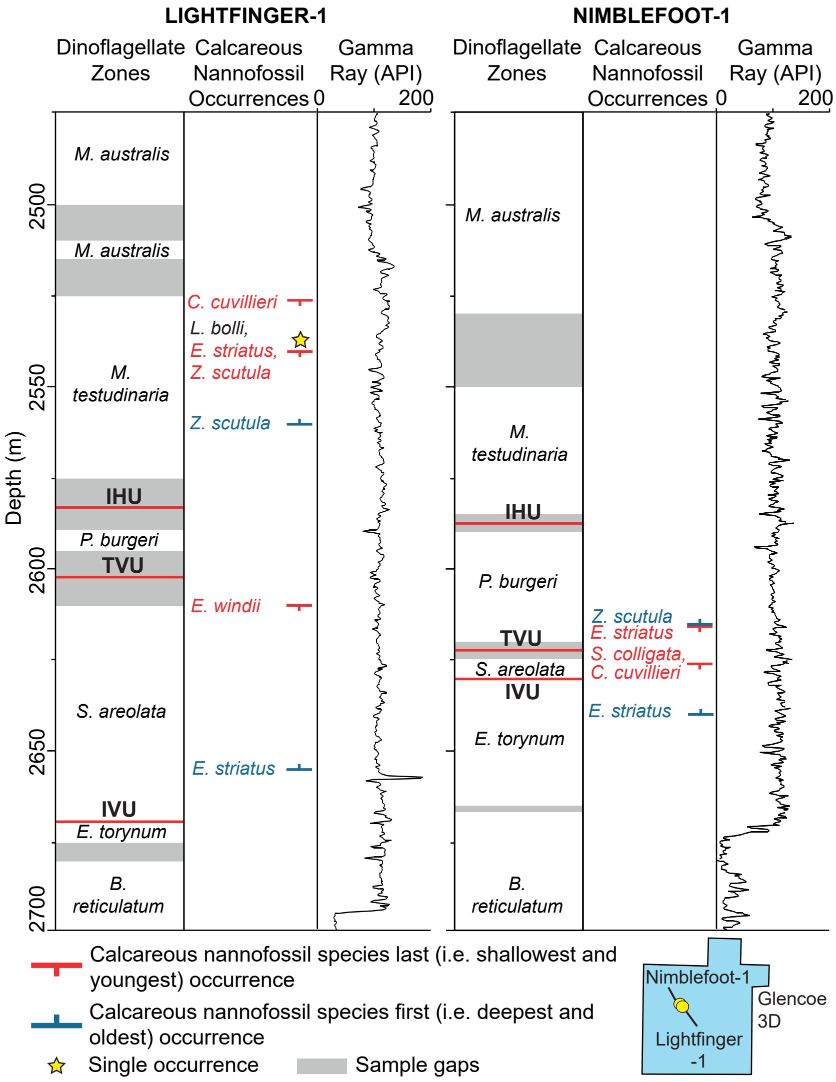

LIGHTFINGER-1
NIMBLEFOOT-1
Dinoflagellate Zones
Calcareous Nannofossil Occurrences
Gamma Ray (API)
0
200
Depth (m)
2500
2550
2600
2650
2700
M. australis
M. testudinaria
IHU
P. burgeri
TVU
S. areolata
IVU
E. torynum
B. reticulatum
C. cuvillieri
L. bolli,
E. striatus,
Z. scutula
Z. scutula
E. windii
E. striatus
Z. scutula
E. striatus
S. colligata,
C. cuvillieri
E. striatus
Calcareous nannofossil species last (i.e. shallowest and youngest) occurrence
Calcareous nannofossil species first (i.e. deepest and oldest) occurrence
Single occurrence
Sample gaps
Nimblefoot-1
Lightfinger -1
Glencoe 3D

Figure 7

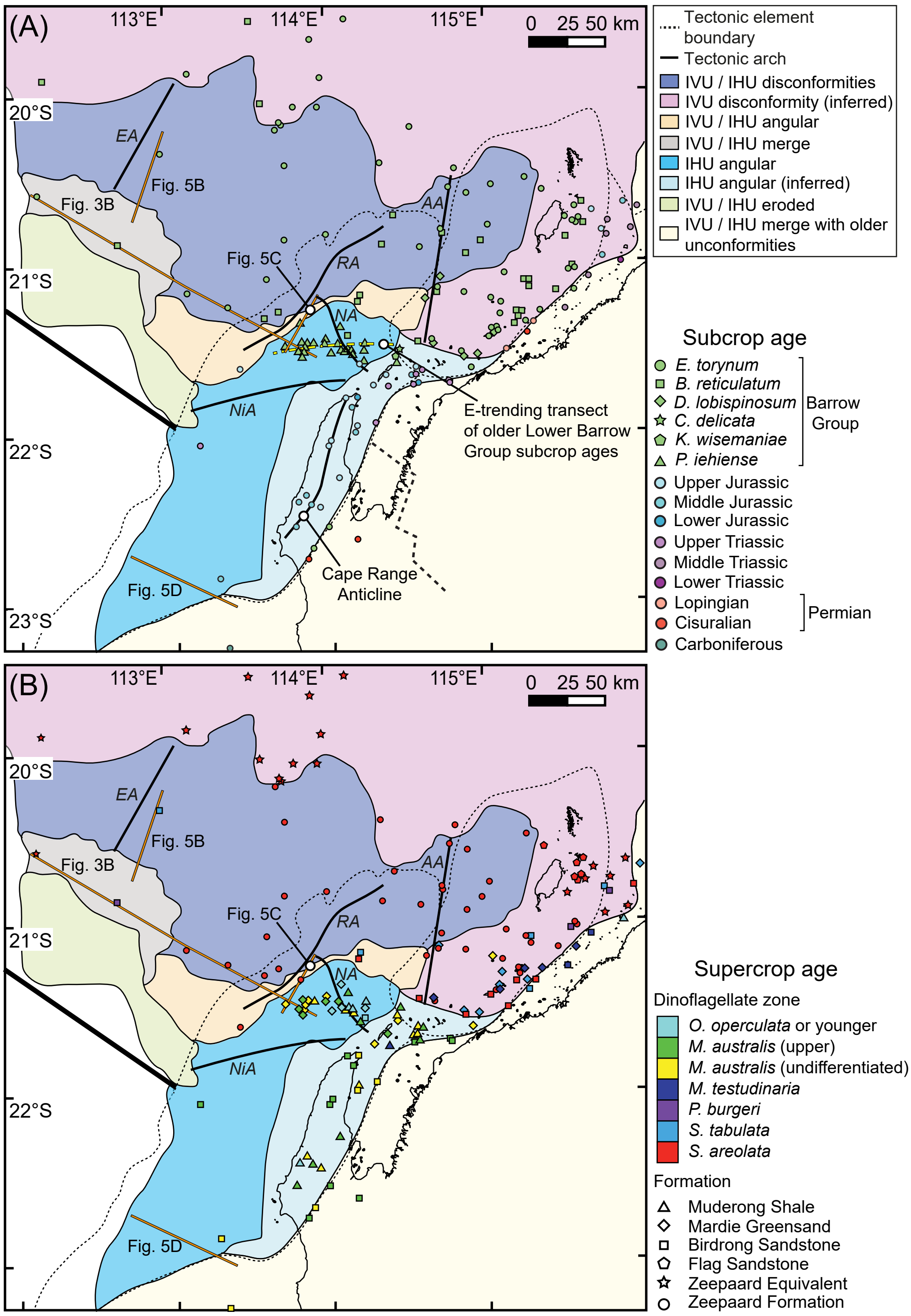

(A)
113°E
114°E
115°E
0 25 50 km
20°S
21°S
22°S
23°S
EA
AA
RA
NA
NiA
Fig. 3B
Fig. 5B
Fig. 5C
Fig. 5D
E-trending transect of older Lower Barrow Group subcrop ages
Cape Range Anticline
Tectonic element boundary
Tectonic arch
IVU / IHU disconformities
IVU disconformity (inferred)
IVU / IHU angular
IVU / IHU merge
IHU angular
IHU angular (inferred)
IVU / IHU eroded
IVU / IHU merge with older unconformities
Subcrop age
E. torynum
B. reticulatum
D. lobispinosum
C. delicata
K. wisemaniae
P. iehiense
Barrow Group
Upper Jurassic
Middle Jurassic
Lower Jurassic
Upper Triassic
Middle Triassic
Lower Triassic
Lopingian
Cisuralian
Permian
Carboniferous
(B)
Supercrop age
Dinoflagellate zone
O. operculata or younger
M. australis (upper)
M. australis (undifferentiated)
M. testudinaria
P. burgeri
S. tabulata
S. areolata
Formation
Muderong Shale
Mardie Greensand
Birdrong Sandstone
Flag Sandstone
Zeepaard Equivalent
Zeepaard Formation

Figure 8

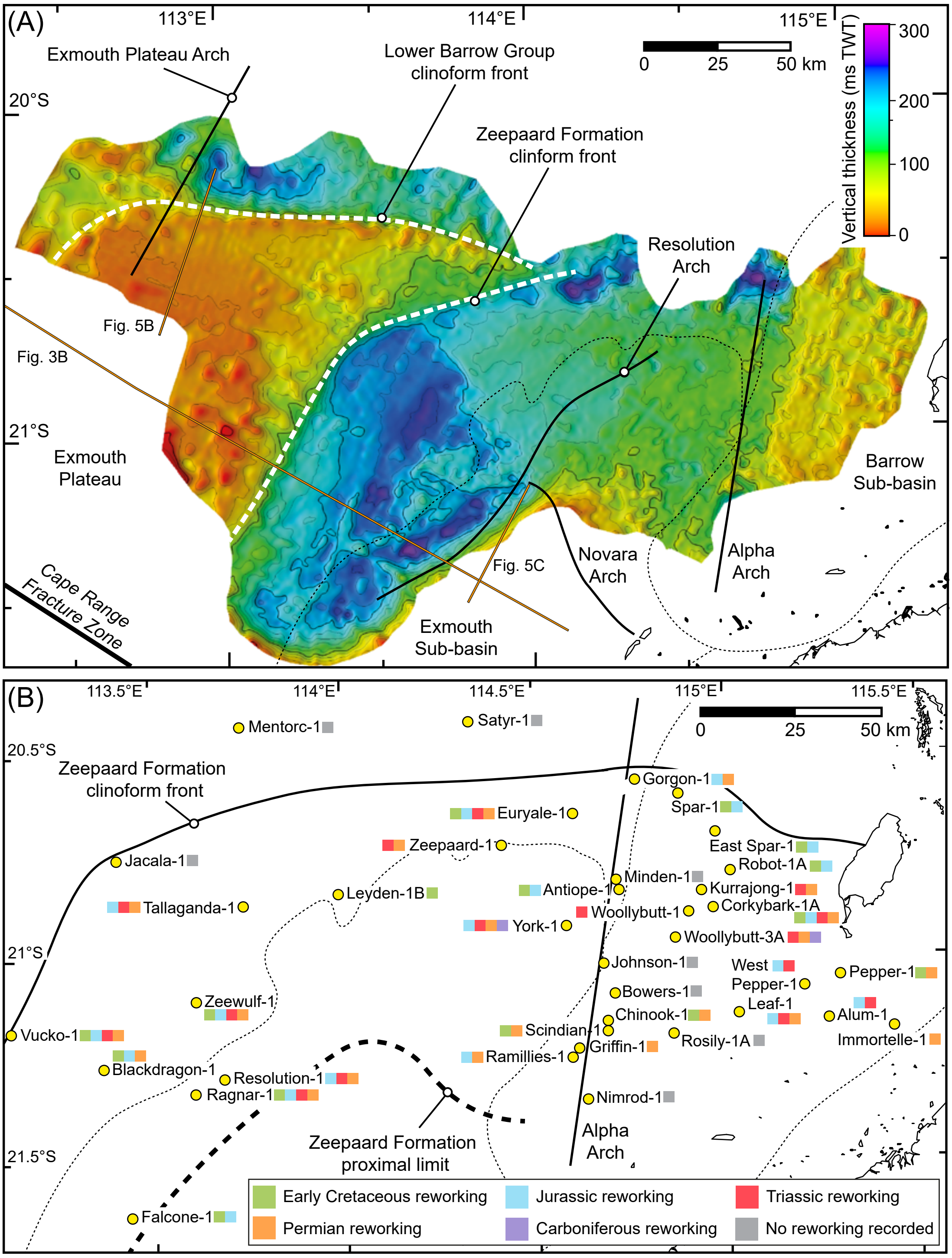
(A)
113°E
114°E
115°E
Exmouth Plateau Arch
Lower Barrow Group
clinoform front
Zeepaard Formation
clinform front
0 25 50 km
Vertical thickness (ms TWT)
300
200
100
0
20°S
21°S
Resolution
Arch
Fig. 5B
Fig. 3B
Exmouth
Plateau
Barrow
Sub-basin
Novara
Arch
Alpha
Arch
Fig. 5C
Cape Range
Fracture Zone
Exmouth
Sub-basin
(B)
113.5°E
114°E
114.5°E
115°E
115.5°E
20.5°S
21°S
21.5°S
0 25 50 km
Mentorc-1
Satyr-1
Zeepaard Formation
clinoform front
Gorgon-1
Spar-1
Euryale-1
East Spar-1
Zeepaard-1
Robot-1A
Jacala-1
Minden-1
Kurrajong-1
Leyden-1B
Antiope-1
Corkybark-1A
Tallaganda-1
Woollybutt-1
York-1
Woollybutt-3A
Johnson-1
West
Pepper-1
Pepper-1
Bowers-1
Zeewulf-1
Leaf-1
Chinook-1
Alum-1
Vucko-1
Scindian-1
Rosily-1A
Immortelle-1
Griffin-1
Blackdragon-1
Ramillies-1
Resolution-1
Ragnar-1
Nimrod-1
Zeepaard Formation
proximal limit
Alpha
Arch
Falcone-1
Early Cretaceous reworking
Jurassic reworking
Triassic reworking
Permian reworking
Carboniferous reworking
No reworking recorded

Figure 9

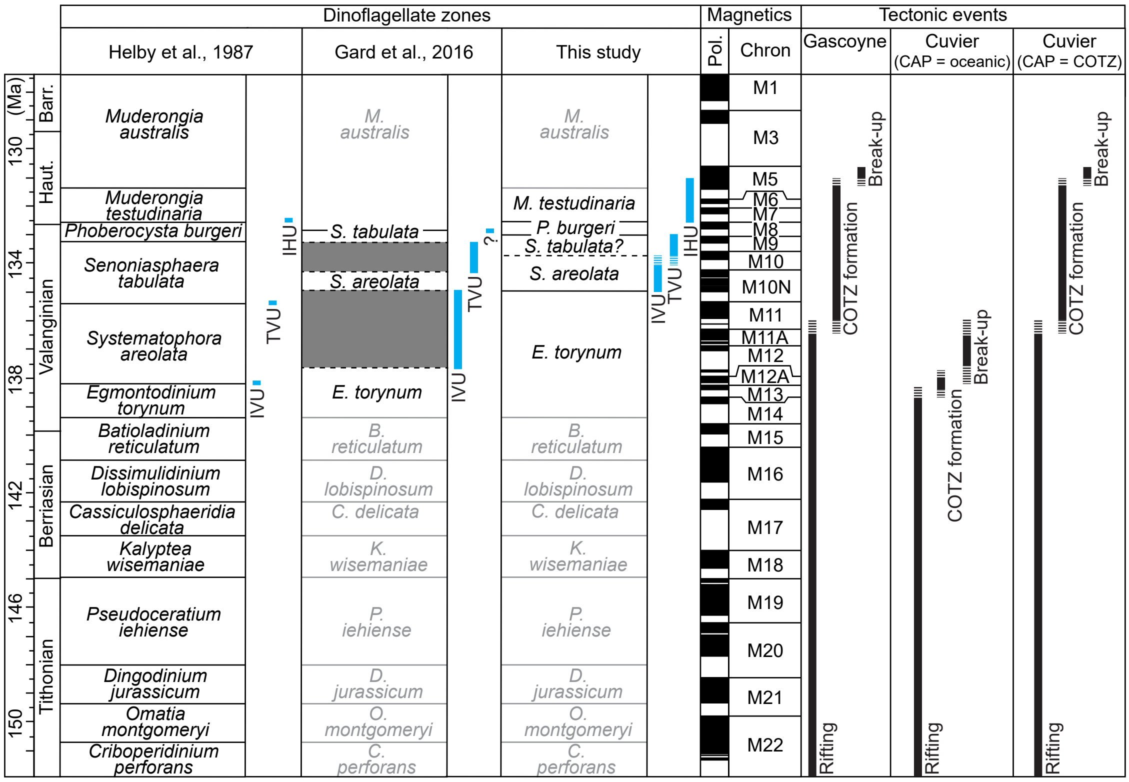

Dinoflagellate zones
Magnetics
Tectonic events
Helby et al., 1987
Gard et al., 2016
This study
Pol.
Chron
Gascoyne
Cuvier (CAP = oceanic)
Cuvier (CAP = COTZ)
(Ma)
130
134
138
142
146
150
Barr.
Haut.
Valanginian
Berriasian
Tithonian
Muderongia australis
Muderongia testudinaria
Phoberocysta burgeri
Senoniasphaera tabulata
Systematophora areolata
Egmontodinium torynum
Batioladinium reticulatum
Dissimulidinium lobispinosum
Cassiculosphaeridia delicata
Kalyptea wisemaniae
Pseudoceratium iehiense
Dingodinium jurassicum
Omatia montgomeryi
Cribroperidinium perforans
IHU
TVU
IVU
M. australis
S. tabulata
S. areolata
E. torynum
B. reticulatum
D. lobispinosum
C. delicata
K. wisemaniae
P. iehiense
D. jurassicum
O. montgomeryi
C. perforans
?
M. testudinaria
P. burgeri
S. tabulata?
M1
M3
M5
M6
M7
M8
M9
M10
M10N
M11
M11A
M12
M12A
M13
M14
M15
M16
M17
M18
M19
M20
M21
M22
Break-up
COTZ formation
Rifting

Figure 10

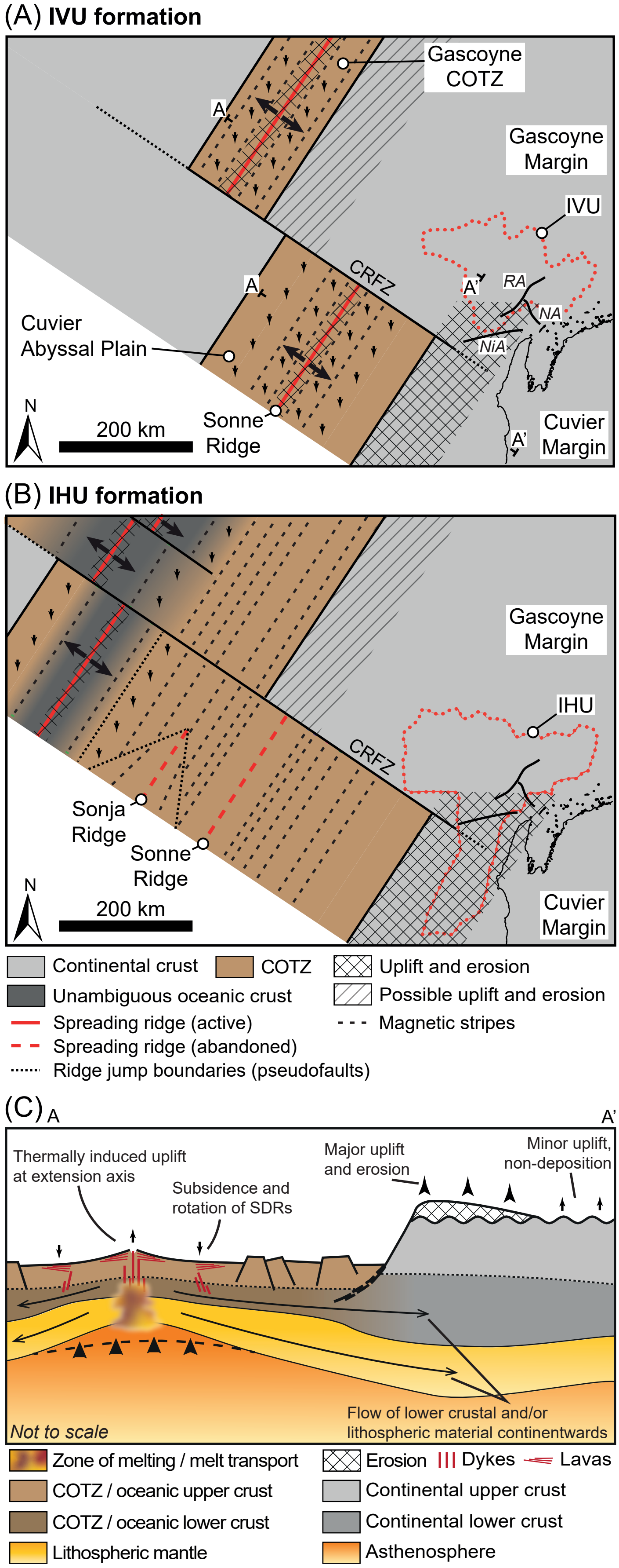

(A) IVU formation
Gascoyne COTZ
Gascoyne Margin
IVU
A
A'
RA
NA
NiA
CRFZ
Cuvier Abyssal Plain
Sonne Ridge
Cuvier Margin
N
200 km
(B) IHU formation
Gascoyne Margin
IHU
CRFZ
Sonja Ridge
Sonne Ridge
Cuvier Margin
N
200 km
Continental crust
COTZ
Uplift and erosion
Unambiguous oceanic crust
Possible uplift and erosion
Spreading ridge (active)
Magnetic stripes
Spreading ridge (abandoned)
Ridge jump boundaries (pseudofaults)
(C) A
A'
Thermally induced uplift at extension axis
Subsidence and rotation of SDRs
Major uplift and erosion
Minor uplift, non-deposition
Flow of lower crustal and/or lithospheric material continentwards
Not to scale
Zone of melting / melt transport
Erosion
Dykes
Lavas
COTZ / oceanic upper crust
Continental upper crust
COTZ / oceanic lower crust
Continental lower crust
Lithospheric mantle
Asthenosphere

Supplementary Table 1: Breakup unconformity locations and reference sources shown in Figure 1

Number	Locality	Reference
1	North Carnarvon Basin	Romine & Durrant (1996)
2	Carnarvon Terrace	Mihut & Müller (1998)
3	Perth Basin	Song & Cawood (2000)
4	Otway Basin	Veevers (1986)
5	Bight Basin	Veevers (1986)
6	Great South Basin	Laird & Bradshaw (2004)
7	Northern Australia	Pigram & Panggabean (1984)
8	Bonaparte Basin	Frankowicz & McClay (2010)
9	Browse Basin	Baillie et al. (1994)
10	NW Borneo	Franke et al. (2014)
11	SW Palawan	Franke et al. (2014)
12	Reed Bank	Franke et al. (2014)
13	NW Palawan	Franke et al. (2014)
14	Cuu Long Basin	Fyhn et al. (2009)
15	Phu Khanh Basin	Franke et al. (2014)
16	Qiongdongnan Basin	Franke et al. (2014)
17	South China Sea	Zhou et al. (1995)
18	Outer Pearl River Mouth Basin	Franke et al. (2014)
19	Hangjiang Depression	Huang et al. (2001)
20	Laptev Sea	Franke (2013)
21	East India Margin	Haupert et al. (2016)
22	Gulf of Aden	Autin et al. (2010)
23	Mozambique Basin	Mahanjane (2012)
24	Outeniqua Basin	Franke (2013)
25	Orange Basin	Franke (2013)
26	Walvis Basin	Franke (2013)
27	Walvis Ridge	Franke (2013)
28	Benguela Basin	Márton et al. (2000)
29	Kwanza Basin	Márton et al. (2000)
30	Lower Congo Basin	Márton et al. (2000)
31	Southern Gabon	Seranne et al. (1992)
32	Rio Muni Basin	Lawrence et al. (2002)
33	Douala Basin	Lawrence et al. (2002)
34	Offshore Benin	Nemčok et al. (2013)
35	Ivory Coast	Nemčok et al. (2013)
36	Guinea Plateau	Edge (2014)
37	Senegal-Mauritanian Basin	Ndiaye et al. (2016)
38	Tarfaya Margin	Le Roy & Piqué (2001)
39	Essaouira Basin	Hafid (2000)
40	Iberian Basin	Tucholke et al. (2007)
41	Armorican Basin	Thinon et al. (2003)
42	Gulf of Lions	Gorini et al. (1993)
43	Western Alps	Claudel & Dumont (1999)
44	Hatton Basin	Vogt et al. (1998)
45	Vøring Margin	Skogseid et al. (1992)
46	Sørvestsnaget Basin	Vagnes (1997)
47	SE Greenland Margin	Larsen & Saunders (1998)
48	Kangerlussuaq Basin	Larsen & Saunders (1998)
49	Baffin Bay	Jackson et al. (1992)
50	Amerasia Basin	Embry & Dixon (1990)
51	Beaufort Sea	Lane (2002)
52	Labrador Margin	Chian et al. (1995)
53	Orphan Basin	Dafoe et al. (2017)
54	Newfoundland Margin	Tucholke et al. (2007)
55	Scotian Basin	Withjack et al. (1998)

56	Georges Bank Basin	Withjack et al. (1998)
57	US Central Atlantic Margin	Post et al. (2013)
58	Carolina Trough	Withjack et al. (1998)
59	Baltimore Canyon Trough	Withjack et al. (1998)
60	Florida Escarpment	Pindell et al. (2014)
61	Guyana Basin	Yang & Escalona (2011)
62	Camamu-Almada Basin	Cainelli & Mohriak (1999)
63	Cumuruxatiba Basin	Cainelli & Mohriak (1999)
64	Campos Basin	Cainelli & Mohriak (1999)
65	Santos Basin	Cainelli & Mohriak (1999)
66	Pelotas Basin	Cainelli & Mohriak (1999)
67	Colorado Basin	Franke (2013)
68	Rawson Basin	Franke (2013)
69	San Jorge Basin	Franke (2013)
70	North Falkland Basin	Franke (2013)
71	Prydz Bay	Stagg (1985)
72	Wilkes Land Margin	Eittreim et al. (1985)

References

Autin, J., Leroy, S., Beslier, M.-O., d'Acremont, E., Razin, P., Ribodetti, A., Bellahsen, N., Robin, C., *et al.* 2010. Continental break-up history of a deep magma-poor margin based on seismic reflection data (northeastern Gulf of Aden margin, offshore Oman). *Geophysical Journal International*, **180**, 501-519.

Baillie, P., Powell, C.M., Li, Z.-X. & Ryall, A. 1994. The tectonic framework of Western Australia's Neoproterozoic to Recent sedimentary basins. *The Sedimentary Basins of Western Australia: Proceedings of the Petroleum Exploration Society of Australia Symposium*. Petroleum Exploration Society of Australia Perth, Australia, 62.

Cainelli, C. & Mohriak, W.U. 1999. Some remarks on the evolution of sedimentary basins along the Eastern Brazilian continental margin. *Episodes - News magazine of the International Union of Geological Sciences*, **22**, 206-216.

Chian, D., Louden, K.E. & Reid, I. 1995. Crustal structure of the Labrador Sea conjugate margin and implications for the formation of nonvolcanic continental margins. *Journal of Geophysical Research: Solid Earth*, **100**, 24239-24253.

Claudel, M. & Dumont, T. 1999. A record of multistage continental break-up on the Briançonnais marginal plateau (Western Alps): Early and Middle-Late Jurassic rifting. *Eclogae Geologicae Helvetiae*, **92**, 45-61.

Dafoe, L.T., Keen, C.E., Dickie, K. & Williams, G.L. 2017. Regional stratigraphy and subsidence of Orphan Basin near the time of breakup and implications for rifting processes. *Basin Research*, **29**, 233-254.

Edge, R. 2014. *Rifting of the Guinea Margin in the Equatorial Atlantic from 112 to 84 Ma: Implications of Paleo-reconstructions for Structure and Sea-surface Circulation.* PhD thesis, University of Arizona.

Eittreim, S.L., Hampton, M.A. & Childs, J.R. 1985. Seismic-reflection signature of Cretaceous continental breakup on the Wilkes Land margin, Antarctica. *Science*, **229**, 1082-1084.

Embry, A.F. & Dixon, J. 1990. The breakup unconformity of the Amerasia Basin, Arctic Ocean: evidence from arctic Canada. *Geological Society of America Bulletin*, **102**, 1526-1534.

Franke, D. 2013. Rifting, lithosphere breakup and volcanism: Comparison of magma-poor and volcanic rifted margins. *Marine and petroleum geology*, **43**, 63-87.

Franke, D., Savva, D., Pubellier, M., Steuer, S., Mouly, B., Auxietre, J.-L., Meresse, F. & Chamot-Rooke, N. 2014. The final rifting evolution in the South China Sea. *Marine and petroleum geology*, **58**, 704-720.

Frankowicz, E. & McClay, K. 2010. Extensional fault segmentation and linkages, Bonaparte Basin, outer North west shelf, Australia. *AAPG Bulletin*, **94**, 977-1010.

Fyhn, M.B., Nielsen, L.H., Boldreel, L.O., Thang, L.D., Bojesen-Koefoed, J., Petersen, H.I., Huyen, N.T., Duc, N.A., *et al.* 2009. Geological evolution, regional perspectives and hydrocarbon potential of the northwest Phu Khanh Basin, offshore Central Vietnam. *Marine and petroleum geology*, **26**, 1-24.

Gorini, C., Le Marrec, A. & Mauffret, A. 1993. Contribution to the structural and sedimentary history of the Gulf of Lions (western Mediterranean) from the ECORS profiles, industrial seismic profiles and well data. *Bulletin de la Société géologique de France*, **164**, 353-363.

Hafid, M. 2000. Triassic–early Liassic extensional systems and their Tertiary inversion, Essaouira Basin (Morocco). *Marine and petroleum geology*, **17**, 409-429.

Haupert, I., Manatschal, G., Decarlis, A. & Unternehr, P. 2016. Upper-plate magma-poor rifted margins: Stratigraphic architecture and structural evolution. *Marine and petroleum geology*, **69**, 241-261.

Huang, C.-Y., Xia, K., Yuan, P.B. & Chen, P.-G. 2001. Structural evolution from Paleogene extension to Latest Miocene-Recent arc-continent collision offshore Taiwan: comparison with on land geology. *Journal of Asian Earth Sciences*, **19**, 619-638.

Jackson, H.R., Dickie, K. & Marillier, F. 1992. A seismic reflection study of northern Baffin Bay: implication for tectonic evolution. *Canadian Journal of Earth Sciences*, **29**, 2353-2369.

Laird, M. & Bradshaw, J. 2004. The break-up of a long-term relationship: the Cretaceous separation of New Zealand from Gondwana. *Gondwana Research*, **7**, 273-286.

Lane, L.S. 2002. Tectonic evolution of the Canadian Beaufort Sea–Mackenzie Delta region: a brief review. *Canadian Society of Exploration Geophysicists Recorder*, **27**, 49-56.

Larsen, H. & Saunders, A. 1998. 41. Tectonism and volcanism at the Southeast Greenland rifted margin: a record of plume impact and later continental rupture. *Proceedings of the Ocean Drilling Program, Scientific Results*, 503-533.

Lawrence, S.R., Munday, S. & Bray, R. 2002. Regional geology and geophysics of the eastern Gulf of Guinea (Niger Delta to Rio Muni). *The Leading Edge*, **21**, 1112-1117.

Le Roy, P. & Piqué, A. 2001. Triassic–Liassic Western Moroccan synrift basins in relation to the Central Atlantic opening. *Marine Geology*, **172**, 359-381.

Mahanjane, E.S. 2012. A geotectonic history of the northern Mozambique Basin including the Beira High–a contribution for the understanding of its development. *Marine and petroleum geology*, **36**, 1-12.

Márton, E., Kuhlemann, J., Frisch, W. & Dunkl, I. 2000. Miocene rotations in the Eastern Alps—palaeomagnetic results from intramontane basin sediments. *Tectonophysics*, **323**, 163-182.

Mihut, D. & Müller, R.D. 1998. Volcanic margin formation and Mesozoic rift propagators in the Cuvier Abyssal Plain off Western Australia. *Journal of Geophysical Research*, **103**, 27135-27127,27149.

Ndiaye, M., Ngom, P.M., Gorin, G., Villeneuve, M., Sartori, M. & Medou, J. 2016. A new interpretation of the deep-part of Senegal-Mauritanian Basin in the Diourbel-Thies area by integrating seismic, magnetic, gravimetric and borehole data: Implication for petroleum exploration. *Journal of African Earth Sciences*, **121**, 330-341.

Nemčok, M., Henk, A., Allen, R., Sikora, P. & Stuart, C. 2013. Continental break-up along strike-slip fault zones; observations from the Equatorial Atlantic. *Geological Society, London, Special Publications*, **369**, 537-556.

Pigram, C. & Panggabean, H. 1984. Rifting of the northern margin of the Australian continent and the origin of some microcontinents in eastern Indonesia. *Tectonophysics*, **107**, 331-353.

Pindell, J., Graham, R. & Horn, B. 2014. Rapid outer marginal collapse at the rift to drift transition of passive margin evolution, with a Gulf of Mexico case study. *Basin Research*, **26**, 701-725.

Post, P.J., Elliott, E.T., Klazynski, R.J., Klocek, E.S., Decort, T.M., Riches, T.J. & Li, K. 2013. US central Atlantic: new plays and petroleum prospectivity. *Geological Society, London, Special Publications*, **369**, 323-336.

Romine, K. & Durrant, J. 1996. Tectonic events, sequence stratigraphy and prediction of petroleum play elements in the Cretaceous and Tertiary of the northern Carnarvon Basin, north west shelf, Australia. *AAPG Bulletin*, **5**.

Seranne, M., Seguret, M. & Fauchier, M. 1992. Seismic super-units and post-rift evolution of the continental passive margin of southern Gabon. *Bulletin de la Société géologique de France*, **163**, 135-146.

Skogseid, J., Pedersen, T., Eldholm, O. & Larsen, B.T. 1992. Tectonism and magmatism during NE Atlantic continental break-up: the Voring Margin. *Geological Society, London, Special Publications*, **68**, 305-320, http://doi.org/10.1144/gsl.sp.1992.068.01.19.

Song, T. & Cawood, P.A. 2000. Structural styles in the Perth Basin associated with the Mesozoic break-up of Greater India and Australia. *Tectonophysics*, **317**, 55-72.

Stagg, H. 1985. The structure and origin of Prydz Bay and MacRobertson shelf, East Antarctica. *Tectonophysics*, **114**, 315-340.

Thinon, I., Matias, L., Réhault, J.-P., Hirn, A., Fidalgo-González, L. & Avedik, F. 2003. Deep structure of the Armorican Basin (Bay of Biscay): a review of Norgasis seismic reflection and refraction data. *Journal of the Geological Society*, **160**, 99-116.

Tucholke, B., Sawyer, D. & Sibuet, J.-C. 2007. Breakup of the Newfoundland–Iberia rift. *Geological Society, London, Special Publications*, **282**, 9-46.

Vagnes, E. 1997. Uplift at thermo-mechanically coupled ocean–continent transforms: modeled at the Senja Fracture Zone, southwestern Barents Sea. *Geo-Marine Letters*, **17**, 100-109.

Veevers, J. 1986. Breakup of Australia and Antarctica estimated as mid-Cretaceous (95±5 Ma) from magnetic and seismic data at the continental margin. *Earth and Planetary Science Letters*, **77**, 91-99.

Vogt, U., Makris, J., O'Reilly, B.M., Hauser, F., Readman, P.W., Jacob, A.B. & Shannon, P.M. 1998. The Hatton Basin and continental margin: crustal structure from wide-angle seismic and gravity data. *Journal of Geophysical Research: Solid Earth*, **103**, 12545-12566.

Withjack, M.O., Schlische, R.W., Olsen, P.E. & Zhang, Q. 1998. Diachronous rifting, drifting, and inversion on the passive margin of central eastern North America: an analog for other passive margins. *AAPG Bulletin*, **82**, 817-835.

Yang, W. & Escalona, A. 2011. Tectonostratigraphic evolution of the Guyana Basin. *AAPG Bulletin*, **95**, 1339-1368.

Zhou, D., Ru, K. & Chen, H.-z. 1995. Kinematics of Cenozoic extension on the South China Sea continental margin and its implications for the tectonic evolution of the region. *Tectonophysics*, **251**, 161-177.